ESC European Society of Cardiology

Cardiovascular Research (2021) **117**, 1489–1509
doi:10.1093/cvr/cvaa244

Role of R-spondin 2 in arterial lymphangiogenesis and atherosclerosis

Bhupesh Singla [1]*, Hui-Ping Lin [1], Alex Chen [2], WonMo Ahn [1], Pushpankur Ghoshal[1], Mary Cherian-Shaw[1], Joseph White[3], Brian K. Stansfield [1,4], and Gábor Csányi[1,5]*

[1]Vascular Biology Center, Medical College of Georgia at Augusta University, 1460 Laney Walker Blvd., Augusta, GA, 30912, USA; [2]Medical Scholars Program, Medical College of Georgia at Augusta University, 1460 Laney Walker Blvd., Augusta, GA, 30912, USA; [3]Department of Pathology, Medical College of Georgia at Augusta University, 1120 15th Street, BF 104, Augusta, GA 30912, USA; [4]Department of Pediatrics, Medical College of Georgia at Augusta University, 1120 15th Street, BI6031, Augusta, GA 30912, USA; and [5]Department of Pharmacology and Toxicology, Medical College of Georgia at Augusta University, 1460 Laney Walker Blvd., Augusta, GA, 30912, USA

Received 2 March 2020; revised 16 July 2020; editorial decision 29 July 2020; accepted 30 July 2020; online publish-ahead-of-print 4 August 2020

Time for primary review: 34 days

Aims Impaired lymphatic drainage of the arterial wall results in intimal lipid accumulation and atherosclerosis. However, the mechanisms regulating lymphangiogenesis in atherosclerotic arteries are not well understood. Our studies identified elevated levels of matrix protein R-spondin 2 (RSPO2) in atherosclerotic arteries. In this study, we investigated the role of RSPO2 in lymphangiogenesis, arterial cholesterol efflux into lesion-draining lymph nodes (LNs) and development of atherosclerosis.

Methods and results The effect of RSPO2 on lymphangiogenesis was investigated using human lymphatic endothelial cells (LEC) *in vitro* and implanted Matrigel plugs *in vivo*. Cellular and molecular approaches, pharmacological agents, and siRNA silencing of RSPO2 receptor LGR4 were used to investigate RSPO2-mediated signalling in LEC. *In vivo* low-density lipoprotein (LDL) tracking and perivascular blockade of RSPO2–LGR4 signalling using LGR4-extracellular domain (ECD) pluronic gel in hypercholesterolemic mice were utilized to investigate the role of RSPO2 in arterial reverse cholesterol transport and atherosclerosis. Immunoblotting and imaging experiments demonstrated increased RSPO2 expression in human and mouse atherosclerotic arteries compared to non-atherosclerotic controls. RSPO2 treatment inhibited lymphangiogenesis both *in vitro* and *in vivo*. LGR4 silencing and inhibition of RSPO2–LGR4 signalling abrogated RSPO2-induced inhibition of lymphangiogenesis. Mechanistically, we found that RSPO2 suppresses PI3K-AKT-endothelial nitric oxide synthase (eNOS) signalling via LGR4 and inhibits activation of the canonical Wnt-β-catenin pathway. ApoE$^{-/-}$ mice treated with LGR4-ECD developed significantly less atherosclerosis compared with control treatment. Finally, increased arterial lymphatic vessel density and improved lymphatic drainage of fluorescently labelled LDL to deep cervical LNs were observed in LGR4-ECD-treated mice.

Conclusion These findings demonstrate that RSPO2 inhibits lymphangiogenesis via LGR4 and downstream impairment of AKT-eNOS-nitric oxide signalling. These results may also inform new therapeutic strategies to promote lymphangiogenesis and improve cholesterol efflux from atherosclerotic arteries.

*Corresponding authors. Tel: +1 706 721 1437; fax: +1 706 721 9799, E-mail: gcsanyi@augusta.edu (G.C.); Tel: +1 706 446 0170; fax: +1 706 721 9799, E-mail: bsingla@augusta.edu (B.S.)

Graphical Abstract

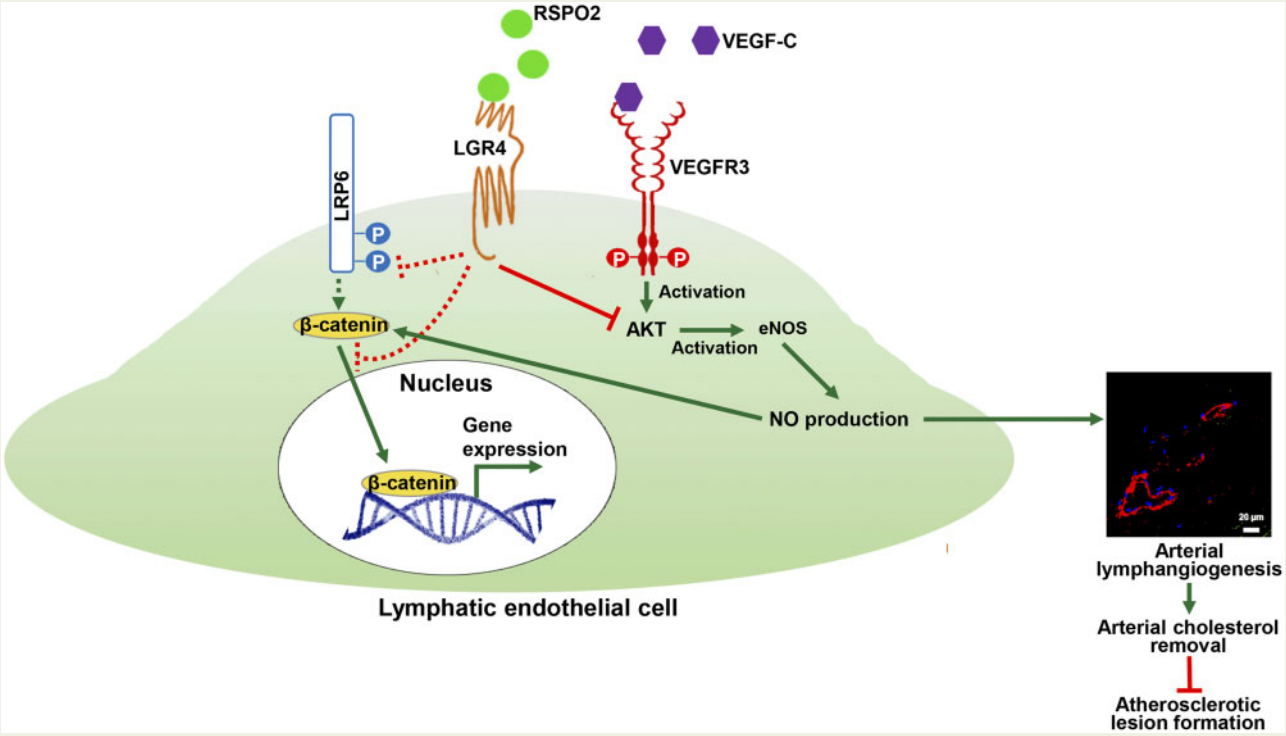

Keywords Atherosclerosis • Lymphangiogenesis • Lymphatic vessel • RSPO2 • LGR4 • Nitric oxide

1. Introduction

Atherosclerotic vascular disease is the underlying cause of myocardial infarction, stable and unstable angina, stroke, and peripheral artery disease.[1] Collectively, these diseases account for the majority of death in the world, and the incidence is continuing to rise because of the international epidemic of obesity, systemic hypertension, diabetes mellitus, and dyslipidaemia, which are all important risk factors for atherosclerosis.[1] Subendothelial retention of plasma-derived apoB containing lipoproteins in large and medium-sized arteries is a critical event that initiates an inflammatory response and promotes the development of atherosclerosis.[2] Atherosclerosis results from the imbalance of arterial influx of plasma lipoproteins through dysfunctional endothelium and the efflux of lipids from the vessel wall via macrophage reverse cholesterol transport (RCT). Macrophage RCT is a multistep process comprising the efflux of cholesterol from macrophage foam cells, HDL-mediated removal of cholesterol from the vessel wall, and its transport to the liver for metabolism and biliary excretion. In recent years, the lymphatic circulation has attracted significant interest in cardiovascular research due to its role in immune cell trafficking, removal of cholesterol-loaded HDL from the periphery via RCT, and regulation of the inflammatory response in general.[3] Immunohistochemistry studies demonstrated the presence of lymphatic vessels (LV) in the adventitial layer of human and rodent atherosclerotic arteries.[4,5] Functional studies identified the lymphatic vasculature as the primary route of cholesterol removal from atherosclerotic vessels via RCT[6] and demonstrated LV-mediated egress of immune cells from atherosclerotic lesions.[7] These results are in line with previous observations demonstrating that arterial segments with dense lymphatic networks are protected from atherosclerosis and that both surgical and genetic disruption of lymphatic drainage promotes atherosclerotic lesion formation.[6–8] Despite this information, the mechanisms and downstream signalling pathways regulating LV formation and macrophage RCT in atherosclerotic arteries are largely unknown.

Vascular endothelial growth factor (VEGF)-C/D-mediated activation of VEGF receptor 3 (VEGFR3) in lymphatic endothelial cells (LEC) promotes lymphangiogenesis via activation of PI3K-AKT, ERK, and endothelial nitric oxide synthase (eNOS) signalling.[9,10] Nitric oxide (NO) derived from eNOS is pivotal for lymphangiogenesis and maintenance of lymphatic function.[11,12]VEGF-C levels are elevated in the adventitia of atherosclerotic arteries.[13] Despite this, adventitial LV regress during the development of atherosclerosis suggesting inhibition of VEGF-C-stimulated lymphangiogenesis in atherosclerotic vessels.[5] Nonetheless, molecular mechanisms that regulate VEGF-C-stimulated signalling in atherosclerotic arteries are largely unknown. Matricellular proteins are a family of structurally unrelated, secretory, and non-structural proteins present in the extracellular matrix, and members of this family are well known for regulating various cellular functions via interacting with cell surface receptors, hormones, proteases, and other signalling molecules.[14] Matrix proteins are expressed at low levels in healthy blood vessels; however, their expression is upregulated in various vascular

Table 1 Demographic and clinical details of human atherosclerotic and non-atherosclerotic cases

Case #	Age/race/sex	Diagnosis	Cause of death
1	88/Caucasian/male	Coronary artery disease	Massive cerebrovascular accident
2	69/Caucasian/female	Coronary artery disease, hypertension, coronary kidney disease	Respiratory failure
3	76/Caucasian/female	Coronary artery disease	Massive bilateral pulmonary embolism and subacute subdural haematoma
4	101/Caucasian/female	Coronary artery disease, aortic stenosis	Congestive heart failure and myocardial infarction
5	51/Caucasian/female	Hypertension, diabetes, atherosclerotic cardiovascular disease, 70–80% obstruction in LAD	Acute on chronic respiratory failure
6	57/African-American/female	Hypertension, atherosclerotic cardiovascular disease, COPD	Hypertensive and atherosclerotic cardiovascular disease
7	57/African-American/male	Oesophageal squamous cells carcinoma, hypertension	Multi-organ failure, coagulopathy, sepsis

COPD, chronic obstructive pulmonary disease; LAD, left anterior descending artery.

pathologies.[15] In preliminary studies, we determined the anti-lymphangiogenic potential of three matricellular proteins, namely thrombospondin-1 (TSP-1), CCN1, and R-spondin 2 (RSPO2). Interestingly, we found that all of these matrix proteins inhibit VEGF-C-stimulated LEC proliferation *in vitro*. Since roles of TSP-1 and CCN1 in atherosclerosis via lymphangiogenesis-independent mechanisms have already been reported,[16,17] the present study was designed to examine the mechanisms by which RSPO2 inhibits lymphangiogenesis and examine its role in the regulation of RCT and development of atherosclerosis.

RSPOs are a family of four secretory proteins (RSPO1 to RSPO4), which function via binding to three cell surface leucine-rich repeat-containing G protein-coupled receptors (LGR4, LGR5, and LGR6).[18–20] Seventeen leucine-rich repeats present on the N-terminal of LGR proteins constitute the extracellular domain (ECD), which has been identified as the binding site for RSPO.[21] These receptors also possess a seven-transmembrane domain typical to G protein-coupled receptors. RSPO1 and RSPO3 have been linked to developmental angiogenesis.[22,23] To our knowledge, the ability of RSPO proteins to regulate lymphangiogenesis has not been studied previously. A recent study demonstrated increased RSPO2 levels in idiopathic pulmonary fibrosis primarily in fibroblasts, which are the predominant cell type in the adventitial layer of large conduit arteries (where LV are present).[24,25] In addition, accumulated evidence suggests the association of RSPO2 with various cancers, including prostate cancer, colon cancer, colorectal cancer, and human Schwann cell tumours,[26] and lymphangiogenesis is a key feature of cancer progression and metastasis.[27] Despite this information, no previous studies have examined the role of RSPO2 in the regulation of lymphangiogenesis and development of atherosclerosis.

In the present study, we sought to examine the role of RSPO2 in lymphangiogenesis *in vitro* and atherosclerotic arterial wall *in vivo*, arterial cholesterol efflux into draining lymph nodes (LNs) and development of atherosclerosis. We observed increased levels of RSPO2 in the adventitial and medial layers of human and mouse atherosclerotic arteries. Mechanistically, we found that RSPO2 inhibits VEGF-C/VEGFR3-mediated signalling in LEC via LGR4, leading to impaired lymphangiogenesis. Downstream of VEGFR3, RSPO2 inhibits PI3K-AKT-eNOS signalling and inhibits activation of the canonical Wnt-β-catenin pathway. Finally, periarterial blockade of RSPO2–LGR4 interaction in hypercholesterolemic mice increased adventitial LV density, improved lymphatic drainage, and attenuated atherosclerotic lesion development *in vivo*. Taken together, these findings may inform new therapeutic strategies to promote arterial lymphangiogenesis and improve cholesterol efflux from atherosclerotic arteries. The results are also expected to stimulate new inquiries into matricellular regulation of lymphangiogenesis in other inflammatory diseases to aid the resolution of inflammation and restoration of tissue homeostasis.

2. Materials and methods

2.1 Reagents and antibodies

Human recombinant RSPO2 and VEGF-C were purchased from Peprotech (Rocky Hill, NJ, USA). Mouse recombinant VEGF-C was obtained from BioLegend (San Diego, CA, USA). EUK-134 and sodium nitroprusside (SNP) were procured from Sigma-Aldrich (St. Louis, MO, USA). Growth factor-reduced Matrigel was obtained from Corning (Bedford, MA, USA). Protease and phosphatase inhibitor cocktail tablets were bought from Roche Diagnostics GmbH (Mannheim, Germany). 2′,7′-Dichlorodihydrofluorescein diacetate (H2DCFDA), diaminofluorescein (DAF)-FM) diacetate, Alexa Fluor 488-phalloidin, Hoechst 33342, and To-Pro 3 were purchased from Life Technologies Corporation (Grand Island, NY, USA). Phospho-eNOS (Ser-1177), phospho-AKT (Ser-473), phospho-ERK1/2 (Thr-202/Tyr-204), phospho-PKCδ (Tyr-311), phospho-low-density lipoprotein receptor-related protein 6 (LRP6) (Ser-1490), total AKT, total ERK1/2, total LRP6, histone 3, and β-catenin antibodies were obtained from Cell Signaling Technology (Danvers, MA, USA). Total eNOS, total PKCδ, VEGFR3, Ki67, GAPDH, and β-actin antibodies were procured from Santa Cruz Biotechnology (Dallas, TX, USA). Lymphatic vessel endothelial hyaluronan receptor-1 (LYVE-1), smooth muscle actin (SMA), vimentin, and TATA-binding protein (TBP) antibodies were purchased from Abcam (Cambridge, MA, USA). Antibodies against RSPO1, RSPO2, and RSPO3 were bought from

Proteintech (Rosemont, IL, USA). CD68 antibody was obtained from ThermoFisher Scientific (Rockford, IL, USA). Mouse recombinant LGR4 Fc chimaera protein was purchased from R&D Systems (Minneapolis, MN, USA).

2.2 Human atherosclerotic tissue

Human atherosclerotic and non-atherosclerotic control arterial tissue was obtained from five female (51–101 years old) and two male (57 and 88 years old) cadaveric donors. Characterization of cadaveric donors, including age, sex, race, cardiovascular risk factors, co-morbidities, and cause of death is shown in *Table 1*. The presence of atherosclerotic lesions was confirmed by Dr Joseph White, Director of Autopsy Services at Augusta University and Oil Red O (ORO) staining. The study was approved by the Biological Safety Office, Augusta University (BSP# 1458) and conducted in accordance with the guidelines in the Declaration of Helsinki. Written informed consent for use of post-mortem tissue for research purposes on behalf of each case was provided by next of kin.

2.3 Animals

Eight- to 10-week-old male mice were used in the present study. C57BL/6 (wild type, JAX, stock # 000664) mice were used for Matrigel plug assay, LN dissection studies, and primary mouse LEC isolation. All mice were maintained on 12-h dark/12-h light cycles in air-conditioned rooms with access to food and drinking water *ad libitum*. Mice were euthanized by inhalation of 2–3% isoflurane and cardiac exsanguination/cervical dislocation wherever appropriate. ApoE-deficient ($ApoE^{-/-}$) mice (JAX, stock # 002052) were fed a Western diet (TD.88137, Envigo, Indianapolis, IN, USA) to induce atherosclerosis.

2.3.1 Blockade of LGR4-mediated signalling in periarterial tissue

Eight-week-old male $ApoE^{-/-}$ mice underwent partial left carotid artery (LCA) ligation as described previously.[28] Briefly, mice were anaesthetized by isoflurane inhalation (4%) and 2–3% isoflurane via a nose cone was used for maintenance of anaesthesia. The LCA of anaesthetized mouse was exposed, and three of four distal branches of the LCA comprising the external carotid artery, internal carotid artery, and occipital artery were ligated using a 6–0 silk suture (Fine Science Tools, Foster City, CA, USA). Immediately after ligation, the LCA was separated from surrounding tissues to disrupt the efferent lymphatic flow, and 50 µL of pluronic F-127 gel containing control protein (IgG) or recombinant LGR4 Fc chimaera protein (200 µg/mL) (LGR4-ECD) applied around the LCA and allowed to solidify for 30 s. Then, the incision site was closed with wound clips (Fine Science Tools). The pluronic solution of control and LGR4-ECD protein was prepared by mixing 100 µL protein solution (500 µg/mL) with 150 µL of 35% pluronic F-127 (Sigma-Aldrich) solution in sterile ice-cold phosphate buffered saline (PBS).[29] Mice were started on a Western diet feeding 5 days before surgery and continued for another 3 weeks post-surgery.

After 3 weeks, whole-body fat, lean mass (Bruker Minispec Live Mice Analyzer, LF90), and fasting blood glucose (ReliOn Prime Blood Glucose Monitoring System) were determined. To evaluate LV-mediated removal of low-density lipoprotein (LDL) from the LCA to periarterial draining LNs *in vivo*, mice were given a retro-orbital injection of Dil-LDL (70 µg) 24 h before sacrifice. Blood was collected from mice 4 and 8 h after injection and at sacrifice using tail snips to determine plasma levels of Dil-LDL. Finally, mice were anaesthetized by isoflurane inhalation (2–3%) and blood was collected in a heparinized syringe via cardiac puncture for lipid analysis. Following euthanasia (as described above), LCA-draining deep cervical LNs and skin-draining inguinal LNs were isolated, digested in RIPA buffer, and DiI fluorescence (excitation: 549 nm and emission: 565 nm) quantified using a Clariostar Monochromator Microplate Reader. DiI fluorescence measured in the plasma of $ApoE^{-/-}$ mice not injected with DiI-LDL was used to determine background fluorescence. Mouse aortic arch with LCA, right carotid artery (RCA), spleen, and liver were isolated and fixed in the Image-iT^{TM} Fixative Solution (Life Technologies Corporation, Grand Island, NY, USA) overnight in dark, and processed for further analysis. Plasma total cholesterol levels were determined by the Amplex Red cholesterol assay (Molecular Probes, Eugene, OR, USA).

2.3.2 LN dissection

Male C57BL/6 mice were injected with proprotein convertase subtilisin/kexin type 9 (PCSK9)-adeno-associated virus 8 (3.97×10^{11} GC) with a liver-specific promoter. PCSK9 is a secretory protein that causes lysosomal degradation of low-density lipoprotein receptor (LDLR) in the liver and induces hypercholesterolaemia.[30] The mice underwent partial LCA ligation procedure as described above, dissection of the LCA-draining deep cervical LN, and fed a Western diet for 4 weeks.[7] Sham-operated mice (LCA ligation, no LN removal) served as controls. Body weight, fasting blood glucose, plasma total cholesterol, and atherosclerotic lesion area in LCA were investigated as described below.

All experimental procedures involving animals were approved by the Institutional Animal Care and Use Committee of Augusta University and conducted in accordance with the National Institutes of Health Guide for the Care and Use of Laboratory Animals.

2.4 Cell culture

Primary human dermal LEC (PromoCell GmbH, Heidelberg, Germany) were cultured in endothelial cell growth medium MV 2 (PromoCell) containing 5% heat-inactivated foetal bovine serum (FBS), 100 IU/mL of penicillin, 100 µg/mL streptomycin, and growth factors bullet kit provided by PromoCell. Cells were maintained in a humidified incubator at 37°C and used till passage 7.

Primary mouse LEC were isolated from C57BL/6 mouse lungs. Mouse lungs were finely minced and digested with collagenase type 2 (1 mg/mL) for 1 h at 37°C. The obtained cell suspension was filtered through a 70 µm cell strainer (Fisherbrand). Sheep anti-rabbit Dynabeads (Life Technologies) coated with LYVE-1 antibodies were used to isolate LYVE-1 positive LEC using a magnetic stand. Isolated LYVE-1 positive cells were cultured in DMEM medium supplemented with 20% FBS, 0.1 mg/mL heparin (Sigma-Aldrich), 0.01 mg/mL endothelial cell growth supplement (Sigma), and 0.05 mg/mL gentamycin (GE Healthcare Bio-Sciences, Pittsburgh, PA, USA) on 0.1% gelatin-coated culture plates. Purity of isolated LEC was confirmed by immunostaining for LYVE-1 and VEGFR3 proteins (Supplementary material online, *Figure S7A*).

THP1 macrophages (Sigma, St. Louis, MO, USA), primary human aortic smooth muscle cells (AoSMC, Lonza, Walkersville, MD, USA), and human aortic adventitial fibroblasts (AoAF, Lonza) were grown in recommended cell culture media and conditions.

2.5 Western blot

Tissue/cell lysates were used to perform western blotting as described previously using the Odyssey CLx Infrared Imaging System (Li-Cor

Biosciences, Lincoln, NE, USA).[31] Briefly, Pierce BCA Protein Assay Kit (ThermoFisher Scientific) was utilized to quantify protein concentrations in lysate preparations. Equal amount of proteins (15–20 μg) were separated using SDS-PAGE gels, transferred onto nitrocellulose membranes (Li-Cor Biosciences) and blocked membranes were probed with the following primary antibodies: RSPO1, RSPO2, RSPO3, phospho-eNOS (Ser-1177), total eNOS, phospho-AKT (Ser-473), total AKT, phospho-ERK1/2 (Thr-202/Tyr-204), total ERK1/2, phospho-PKCδ (Tyr-311), total PKCδ, VEGFR3, phospho-LRP6 (Ser-1490), total LRP6, histone 3, TBP, GAPDH, and β-actin. The IRDye-conjugated secondary antibodies (Li-Cor Biosciences) were employed to detect the primary antibodies bound to membranes. The densitometry analysis was done using the NIH Image J software.

2.6 Immunohistochemistry

Lipid deposition was determined using ORO staining as previously described.[28] Briefly, sections were washed with PBS to remove OCT and then incubated with 60% isopropanol, stained with ORO solution (Sigma-Aldrich, 2.0% w/v), and counterstained with haematoxylin and eosin (H&E, Sigma-Aldrich). Images were taken using a phase-contrast microscope.

Frozen sections were washed with PBS and permeabilized with 0.1% Triton X-100 for 15 min. While, paraffin sections were deparaffinized, rehydrated, and boiled in citrate buffer (10 mM, pH 6.0) at 95°C for 10 min to retrieve antigen. Arterial sections were blocked and incubated with primary antibodies against RSPO2, CD68, SMA, vimentin, and LYVE-1 overnight at 4°C in a humidified chamber. Then, sections were washed and incubated with fluorescently labelled secondary antibodies (Jackson ImmunoResearch, West Grove, PA, USA) for 1 h at room temperature, followed by DAPI/Hoechst 33342/To-Pro 3 staining and mounting with Fluoromount-G (ThermoFisher Scientific). Images were captured using a Zeiss 780 inverted confocal microscope. Image fluorescence analysis was performed with Image-Pro Plus software (Media Cybernetics, Bethesda, MD, USA).

Mouse LCA frozen sections were stained with H&E, Masson's trichrome, and ORO using standard protocols. Sections were also stained using antibodies for CD68 and LYVE-1 to determine macrophage content and LV density, respectively. Immunohistochemical staining was carried out using Lab Vision™ UltraVision™ LP Detection System (ThermoFisher Scientific) according to the manufacturer's instructions.

2.7 LEC proliferation assay

LEC proliferation was measured using the Cell Proliferation Kit I (MTT) from Roche Diagnostics GmbH. Briefly, cells were seeded at a density of 10 000 cells per well in a 96-well plate. Next day, cells were pretreated with vehicle (PBS) or human recombinant RSPO2 (100 ng/mL) in basal medium MV 2 (PromoCell GmbH) containing 0.5% FBS for 6 h, and stimulated with human recombinant VEGF-C (100 ng/mL) for 48 h. Following stimulation, 10 μL MTT labelling reagent was added to each well, and cells were incubated at 37°C for 4 h. The formed purple formazan crystals were solubilized with solubilization buffer overnight, and absorbance measured at 570 nm using Clariostar Monochromator Microplate Reader (BMG Labtech, Cary, NC, USA). Absorbance at 690 nm was taken as reference.

For determination of Ki67 positive cells, LEC were plated on coverslips inserted in a 24-well plate. LEC were pretreated with vehicle or RSPO2 (100 ng/mL) for 6 h and stimulated with VEGF-C (100 ng/mL) for 24 h. Cells were fixed, permeabilized, blocked, and incubated with Ki67 primary antibodies overnight at 4°C. Cells were then incubated with fluorescently labelled secondary antibodies (Jackson ImmunoResearch), Alexa Fluor 488-phalloidin, and To-Pro 3. Images were captured using a Zeiss 780 inverted confocal microscope, and Ki67 positive cells counted using the NIH Image J software.

2.8 LEC transwell migration assay

LEC migration in response to RSPO2 treatment was investigated using transwell inserts with 8 μm pore polycarbonate membranes (Corning, NY, USA) in 24-well plate. Briefly, cells were pretreated with/without RSPO2 for 6 h. After 6 h, 20 000 cells in 100 μL of basal medium MV2 (0.5% FBS) containing VEGF-C in the presence or absence of RSPO2 were seeded in upper chambers, and lower chambers filled with complete endothelial cell growth medium MV 2. After 12 h of incubation at 37°C, cells on the top of membranes were wiped, and membranes were fixed and stained with 0.5% crystal violet. Images of 7–9 randomly selected fields were acquired using an inverted phase-contrast microscope, and the number of cells migrated to the lower side of the membranes determined using the NIH Image J software.

2.9 LEC tube formation assay

A Matrigel tube formation assay was performed as previously described.[32] Briefly, 96-well plates were coated with growth factor-reduced Matrigel for 45 min at 37°C. Then, vehicle- or RSPO2-pretreated LEC (20 000 cells/well) in basal medium MV2 (0.5% FBS) containing VEGF-C with or without RSPO2 were seeded onto solidified Matrigels and incubated for 6 h at 37°C in a humidified incubator with 5% CO_2. Images of tube formation were either captured directly using an inverted phase-contrast microscope or Matrigels were fixed, permeabilized, and stained with Alexa Fluor 488-phalloidin, and images were recorded using an inverted fluorescent microscope. The tube length and number of branching points were measured using the NIH ImageJ software or Tube Formation ACAS Image Analysis software (ibidi, Munich, Germany).

2.10 *In vivo* lymphangiogenesis assay

In vivo lymphangiogenesis was determined using the Matrigel plug assay.[33] Eight- to 10-week-old male wild-type mice on the C57BL/6 background were injected subcutaneously (s.c.) with growth factor-reduced Matrigel premixed with murine VEGF-C (100 ng/mL), VEGF-C + RSPO2 (200 ng/mL), or VEGF-C + RSPO2 + SNP (2 μM). Mice were euthanized by inhalation of 2–3% isoflurane and cervical dislocation after 2 weeks, Matrigel plugs harvested, fixed in 4% paraformaldehyde, and LYVE-1 immunostaining performed. Digital images of staining were taken using a Zeiss 780 inverted confocal microscope.

2.11 Quantitative real-time PCR

Total cellular RNA was extracted from cultured human or mouse LEC employing RNA purification kit (IBI Scientific, Peosta, IA, USA). Reverse transcription was done using 500 ng of RNA with TaqMan® Reverse Transcriptase kit (Applied Biosystems, Carlsbad, CA, USA) as per the manufacturer's instructions. The quantitative real-time PCR (qRT-PCR) was performed with SYBR Green Supermix (Applied Biosystems) in a StepOne Plus system (Applied Biosystems). Relative gene expression was determined with the $\Delta\Delta C_t$ method using GAPDH (human/mouse) as the internal control. The primer sequences used for real-time PCR are shown in Supplementary material online, *Table S1*.

2.12 Gene silencing

A smart pool of siRNA for LGR4 and a non-targeting control siRNA were purchased from Dharmacon (Lafayette, CO, USA). Human LEC were transfected with LGR4 siRNA or control siRNA using the TransIT-TKO transfection reagent (Mirus Bio LLC, Madison, WI, USA) according to the manufacturer's instructions. Gene silencing using siRNA was confirmed by qRT-PCR. Cells were used for further experiments 48 h post-transfection.

2.13 Intracellular NO analysis

Human LEC were plated in a 96-well plate at a density of 10 000 cells/well. Next day, cells were pretreated with vehicle or RSPO2 for 6 h and stimulated with VEGF-C for 1 h. After the incubation time, cells were washed and incubated with DAF-FM diacetate solution (5 μM) for 45 min at 37°C. Then, cells were washed, incubated with fresh basal media without serum for 30 min, and fluorescence measured using excitation/emission spectra 495/515 nm with a Clariostar Monochromator Microplate Reader. L-N^G-Nitro arginine methyl ester (L-NAME) (NO synthetase inhibitor, 100 μM, 1 h)-pretreated cells were used as negative controls.

2.14 Reactive oxygen species generation

Intracellular reactive oxygen species (ROS) were determined using H2DCFDA.[34] Briefly, LEC were seeded in a six-well plate. After overnight attachment, cells were treated with vehicle or RSPO2 for the indicated time points. Cells were then washed and incubated with H2DCFDA (5 μM) for 30 min at 37°C followed by flow cytometry analysis (Ex: 492 nm, Em: 525 nm) using a BD Accuri C6 flow cytometer. Mean fluorescence intensity was used to compare ROS generation between groups.

H_2O_2 production by LEC after RSPO2 exposure was investigated using the Amplex Red assay as described previously.[35] Briefly, LEC were plated in a black 96-well plate (10 000 cells/well). Next day, cells were treated with or without RSPO2 (100 ng/mL) in assay buffer containing 25 mM Hepes (pH 7.4), 0.12 M NaCl, 3 mM KCl, 1 mM $MgCl_2$, 0.1 mM Amplex Red, and 0.032 unit of HRP. Amplex Red fluorescence (excitation 530–560 nm and emission ~590 nm) was measured every 2 min for 120 min at 37°C using a Clariostar Monochromator Microplate Reader.

2.15 β-Catenin nuclear localization

To investigate β-catenin nuclear localization in response to RSPO2 treatment, LEC plated on coverslips were treated with vehicle or RSPO2 (100 ng/mL) for 6 h and stimulated with VEGF-C (100 ng/mL) for 15 min. After that, cells were immunostained for β-catenin and co-stained with nuclear dye Hoechst 33342. Images were taken using a Zeiss 780 inverted confocal microscope. At least five images of randomly chosen microscopic fields per treatment condition per experiment were captured. The co-localization of green (β-catenin) and red (nucleus) colours were determined using Image-Pro Plus software (Media Cybernetics) to investigate nuclear translocation of β-catenin, and values of the co-localization coefficient are shown. Furthermore, cells were treated as indicated and nuclear-cytoplasmic fractionation executed using the NE-PER Nuclear and Cytoplasmic Extraction Reagents (Pierce Biotechnology, Rockford, IL, USA). Western blot experiments were performed employing nuclear and cytoplasmic fractions of LEC.

2.16 Statistical analysis

GraphPad Prism (La Jolla, CA, USA) was utilized to perform statistical analyses. The data are expressed as mean ± SEM. Student's *t*-test and one or two-way ANOVA were used, followed by *post hoc* analysis for multiple comparisons where appropriate. A *P*-value <0.05 was considered statistically significant.

3. Results

3.1 RSPO2 levels are elevated in human and mouse atherosclerotic arteries

Recent reports have demonstrated that RSPO2 protein levels are decreased in colorectal cancer and lung cancer patients and RSPO2 suppresses tumour growth via inhibition of Wnt-β-catenin signalling.[36,37] To determine whether RSPO2 expression is also dysregulated in atherosclerotic tissue, we quantified its expression in human atherosclerotic aorta and non-atherosclerotic control segments from cadaveric donors with and without a history of cardiovascular disorders (CVD). It is well known that disturbed flow with associated reciprocating low shear stress in branch points and curvatures promotes atherosclerosis.[38] In contrast, arterial regions exposed to sustained laminar flow with high shear stress, such as the descending thoracic aorta, are protected from atherosclerosis.[38] ORO staining revealed the presence of atherosclerotic lesions in the inner curvature (IC) of human aortic arch but not in the descending aorta (DA) (*Figure 1A*). Immunoblotting using tissue lysates prepared from human IC and DA demonstrated that RSPO2 levels are increased in human atherosclerotic arteries compared to non-atherosclerotic arterial tissue (*Figure 1B*). Characterization of cadaveric donors, including age, sex, cardiovascular risk factors, co-morbidities, and cause of death is shown in *Table 1*. We also executed western blot experiments to determine the levels of other RSPO isoforms including RSPO1 and RSPO3 in human aortic tissue with or without atherosclerosis. No differences were observed in the expression of RSPO3; however, RSPO1 levels were decreased in atherosclerotic aortic segments compared to non-atherosclerotic control tissue (Supplementary material online, *Figure S1*).

To investigate whether RSPO2 expression is elevated in mouse models of atherosclerosis, 8- to 10-week-old atheroprone $ApoE^{-/-}$ mice were fed a Western diet for 12 weeks, and their aortae were isolated and used for determination of RSPO2 protein levels. ORO staining confirmed atherosclerotic lesions in the IC of $ApoE^{-/-}$ aortic arch but not in the DA (*Figure 1C*). Similar to western blot data obtained using human aortic tissue, RSPO2 levels were significantly increased in $ApoE^{-/-}$ mice atherosclerotic aortae compared with non-atherosclerotic control segments of DA (*Figure 1D*).

Next, we performed immunostaining to determine in which layer(s) of the atherosclerotic arterial wall RSPO2 levels are upregulated. In these experiments, $ApoE^{-/-}$ mice underwent partial LCA ligation and fed a Western diet for 3 weeks. Increased RSPO2 staining in the adventitial layer of mouse atherosclerotic LCA was observed compared with the non-atherosclerotic RCA (*Figure 1E*). Next, we used atherosclerotic and non-atherosclerotic left anterior descending (LAD) coronary arteries from cadaveric donors for immunostaining experiments. Interestingly, we observed increased RSPO2 expression in adventitial and medial layers as well as in the plaque area of human atherosclerotic arteries compared with non-atherosclerotic LAD (*Figure 1F and G*). Additional immunofluorescence experiments were performed using human atherosclerotic LAD arteries, to identify the cell type(s) in the arterial wall

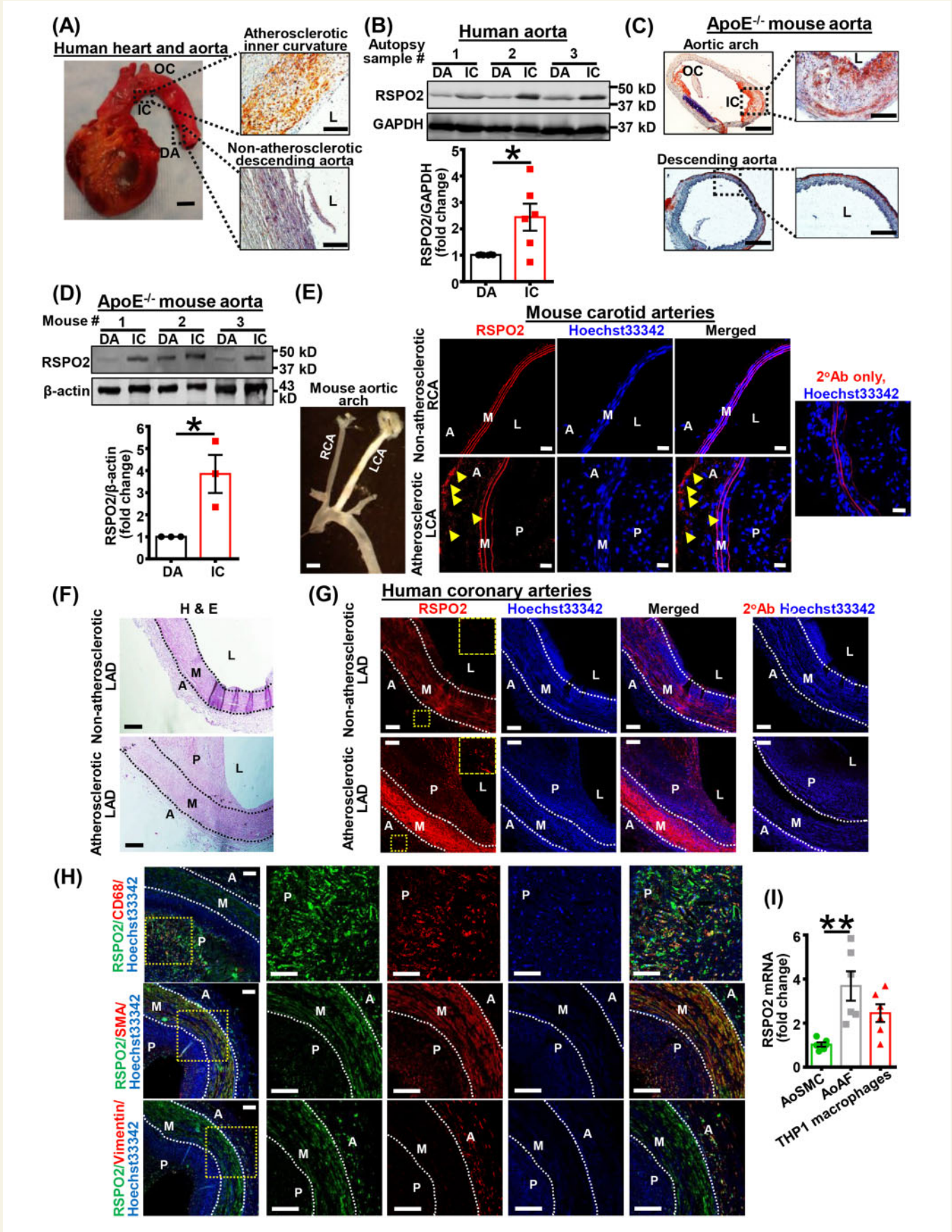

Figure 1 RSPO2 expression is increased in human and mouse atherosclerotic arteries. (*A*) Human aortic tissues were obtained from cadaveric donors (BSP#: 1458). ORO staining of the IC and DA was performed to confirm lipid deposition. Representative of $n = 6$ experiments. Insets indicate tissue isolation sites. Human heart scale bar 2.5 cm; ORO staining scale bar 100 μm. (*B*) Representative western blot images of RSPO2 protein expression in human aortic

expressing RSPO2. Arteries were stained for RSPO2, CD68 (macrophage marker), SMA (SMC marker), and vimentin (fibroblast marker). Our results demonstrated that RSPO2 colocalizes with CD68-positive areas in atherosclerotic lesions (*Figure 1H*). We also found that SMA positive cells and adventitial fibroblasts colocalize with RSPO2 staining in the medial and adventitial layer, respectively (*Figure 1H*). We next performed qRT-PCR experiments to quantify mRNA levels of RSPO2 in human AoSMC, human AoAF, and human macrophages (THP1). The qRT-PCR data exhibited significantly higher levels of RSPO2 in adventitial fibroblasts compared with smooth muscle cells (*Figure 1I*). Although there was a trend, no significant differences in RSPO2 mRNA levels were observed between adventitial fibroblasts and macrophages (*Figure 1I*). Taken together, these data demonstrate that RSPO2 levels are upregulated in multiple areas of atherosclerotic arteries, including the adventitial layer where the lymphatic vasculature is primarily present.[4,5] Despite this information the role of RSPO2 in lymphangiogenesis and the pathogenesis of atherosclerosis in general is not known.

3.2 RSPO2 inhibits lymphangiogenesis *in vitro* and *in vivo*

Previous studies reported that the lymphatic vasculature is the primary route of cholesterol removal from atherosclerotic vessels via mediating RCT.[4–7] Consistent with this statement, Supplementary material online, *Figure S3A–D* demonstrates that disruption of lymphatic drainage by removal of the LCA-draining deep cervical LN stimulates atherosclerotic lesion formation in ApoE$^{-/-}$ mice. LN dissection did not affect body weight, fasting blood glucose, and plasma cholesterol levels (Supplementary material online, *Figure S3E–G*). In animal models and human arteries, LV have been consistently observed in the adventitial and periadventitial regions of the vessel wall.[4,5] Confirming these findings, Supplementary material online, *Figure S2* and *Figure 7N* demonstrate that LV are primarily observed in the adventitial layer of human and rodent atherosclerotic arteries.

As RSPO2 expression was increased in the adventitial layer of atherosclerotic arteries, where LV have been primarily observed, we investigated whether RSPO2 treatment inhibits lymphangiogenesis. First, we examined the effect of RSPO2 treatment on the proliferation of human LEC using MTT assay. As shown in *Figure 2A*, RSPO2 treatment (100 ng/mL, 6 h) significantly inhibited VEGF-C-stimulated (100 ng/mL, 48 h) LEC proliferation. RSPO2 treatment did not induce apoptosis of LEC (Supplementary material online, *Figure S4A*). Next, we performed cell immunofluorescence experiments to quantify Ki67 positive cells following VEGF-C and VEGF-C + RSPO2 treatments. Immunofluorescence results demonstrated a significantly decreased number of Ki67 positive cells in the VEGF-C + RSPO2-treated group compared with control cells exposed to VEGF-C alone (*Figure 2B*). Transwell migration assay data indicated that RSPO2 suppressed VEGF-C-stimulated migration of LEC (*Figure 2C and D*). To further investigate the effect of RSPO2 treatment on the lymphangiogenic ability of LEC, a Matrigel-based tube formation assay was performed. Consistent with LEC proliferation and migration analysis, RSPO2-treated LEC showed reduced tube formation as indicated by decreased tube length and lower number of branching points compared to vehicle-treated cells (*Figure 2E–G*). Taken together, these findings suggest that RSPO2 inhibits LEC proliferation and migration, leading to impaired lymphangiogenesis *in vitro*.

Next, we used the Matrigel plug assay to investigate the ability of RSPO2 to inhibit lymphangiogenesis *in vivo*. Matrigel mixed with VEGF-C with or without RSPO2 was administered s.c. into C57BL/6J mice (*Figure 2H*). Matrigel plugs were harvested 2 weeks after implantation and plug sections stained with anti-LYVE-1 to determine LV density. Immunostaining analysis of plug sections revealed remarkably reduced LYVE-1 positive area in plugs containing VEGF-C + RSPO2 compared with VEGF-C treatment alone (*Figure 2H and I* and Supplementary material online, *Figure S4B*). Consistent with *in vitro* observations, these data suggest the anti-lymphangiogenic potential of RSPO2 *in vivo*.

Figure 1 Continued

tissues from atherosclerotic IC and DA are shown. Bar graph represents mean protein levels along with individual data points calculated using densitometric analysis and expressed as a ratio of RSPO2 to GAPDH ($n = 6$). (*C*) ApoE$^{-/-}$ mice were fed a Western diet for 12 weeks, their aortae were isolated, sectioned, and ORO staining performed. Scale bar 100 μm (left panels) and 50 μm (right panels). Representative images are shown ($n = 3$). (*D*) Representative western blot images of RSPO2 protein expression in the IC and DA segments of ApoE$^{-/-}$ aorta. Bar graph represents mean protein levels along with individual data points and expressed as a ratio of RSPO2 to GAPDH ($n = 3$). (*E*) ApoE$^{-/-}$ mice underwent partial LCA ligation, fed a Western diet for 4 weeks and immunostaining for RSPO2 (red) was performed on cross-sections of the RCA (non-atherosclerotic control) and atherosclerotic LCA. Nuclei were counterstained with Hoechst 33342 (blue). RSPO2 staining is indicated by yellow arrowheads in the adventitial layer ($n = 3$). Scale bar 1 mm (left most panel); 20 μm (immunofluorescence staining). Left panel indicates the presence of atherosclerosis in the LCA, but not in the RCA. (*F*) Haematoxylin and eosin staining demonstrating the presence or absence of atherosclerotic lesions in human LAD arteries. (*G*) Immunofluorescence staining in consecutive human LAD sections was conducted similar to (*E*). Enlarged images of yellow insets are also shown. Representative of $n = 3$ experiments. Black/white dotted lines denote internal and external elastic laminas. Arterial sections stained with fluorescently labelled secondary antibodies (2°Ab) only and Hoechst 33342 were considered as negative controls. Scale bar 100 μm. (*H*) Human atherosclerotic LAD sections were stained with RSPO2, CD68 (macrophage marker), SMA (SMC marker), and vimentin (fibroblast marker). Representative images are shown. Magnified images of yellow insets are also shown ($n = 3$). (*I*) Total RNA was extracted from human AoSMC, AoAF, and THP1 macrophages, and qRT-PCR performed to determine the relative levels of RSPO2. GAPDH was used as an internal control. Bar graph represents mRNA levels of RSPO2 ($n = 6$). Statistical analyses were performed using a two-tailed unpaired *t*-test (*B* and *D*) and one-way ANOVA (*I*). Data represent mean ± SEM. $^*P < 0.05$ and $^{**}P < 0.01$. A, adventitia; AoAF, aortic adventitial fibroblasts; AoSMC, aortic smooth muscle cells; DA, descending aorta; IC, inner curvature; L, lumen; LAD, left anterior descending artery; LCA, left carotid artery; M, media; OC, outer curvature; P, plaque; RCA, right carotid artery; RSPO2, R-spondin 2.

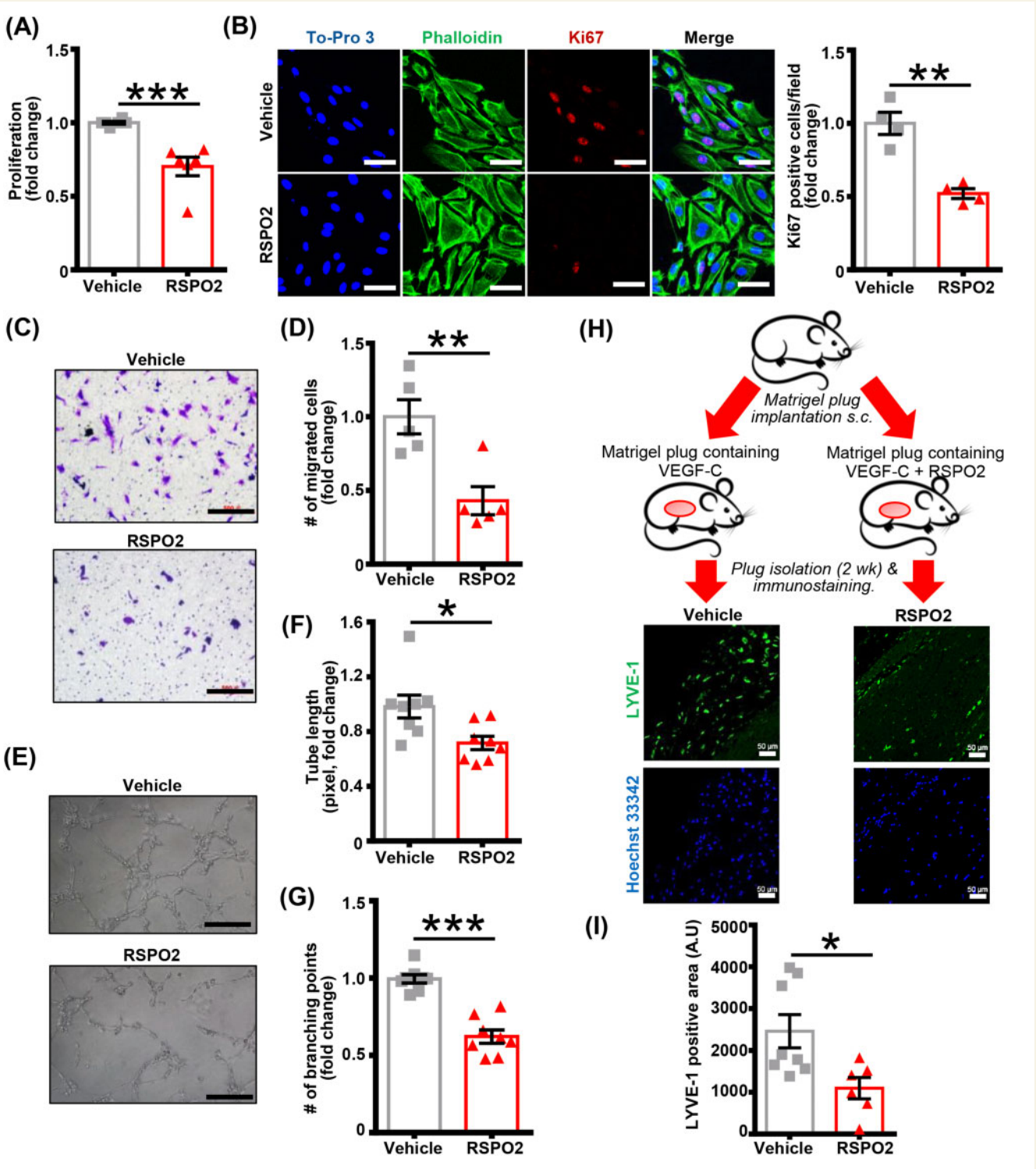

Figure 2 RSPO2 suppresses lymphangiogenesis *in vitro* and *in vivo*. (*A*) Human LEC were pretreated with vehicle or RSPO2 (100 ng/mL) in basal media MV2 containing 0.5% FBS for 6 h, stimulated with VEGF-C (100 ng/mL) and proliferation investigated after 48 h using MTT assay. Data are representative of six independent experiments performed at least in triplicate. (*B*) LEC grown on coverslips were pretreated with vehicle or RSPO2 for 6 h and stimulated with VEGF-C for 24 h. Cells were fixed and immunostained for Ki67 (red). Nuclei and actin filaments were counterstained with To-Pro 3 (blue) and phalloidin (green), respectively. Images were captured from five to nine random fields. Representative images are shown. Scale bar 50 µm. Bar graph represents the mean number of Ki67 positive cells/field ($n = 4$). (*C*) Vehicle or RSPO2-pretreated LEC were seeded in upper chambers of transwell plate in basal medium containing VEGF-C ± RSPO2 and migration investigated after 12 h. Images of seven to nine randomly selected fields were acquired and number of migrated cells counted. Representative photomicrographs are shown. Scale bar 500 µm. (*D*) Bar graph represents the number of migrated cells ($n = 5$). (*E–G*) Vehicle or RSPO2-pretreated LEC were seeded in wells of a Matrigel-coated plate in basal medium containing VEGF-C ± RSPO2 and tube formation determined (6 h). Representative photomicrographs are shown. Scale bar 500 µm (*E*). Images of random fields were taken, and tube length (*F*) and number of branching points (*G*) quantified ($n = 8$). (*H*) Matrigel plugs mixed with either VEGF-C or VEGF-C + RSPO2 were implanted subcutaneously in wild-type mice. Plugs were isolated after 2 weeks, sectioned and immunostained for LYVE-1. (*I*) Quantitative analysis of LYVE-1 in implanted Matrigel plugs. Bar diagram represents mean LYVE-1 positive area ($n = 6–8$). Statistical analyses were performed using a two-tailed unpaired *t*-test. Data represent mean ± SEM. $^{*}P < 0.05$, $^{**}P < 0.01$, and $^{***}P < 0.001$. LYVE-1, lymphatic vessel endothelial hyaluronan receptor-1; RSPO2, R-spondin 2; VEGF, vascular endothelial growth factor.

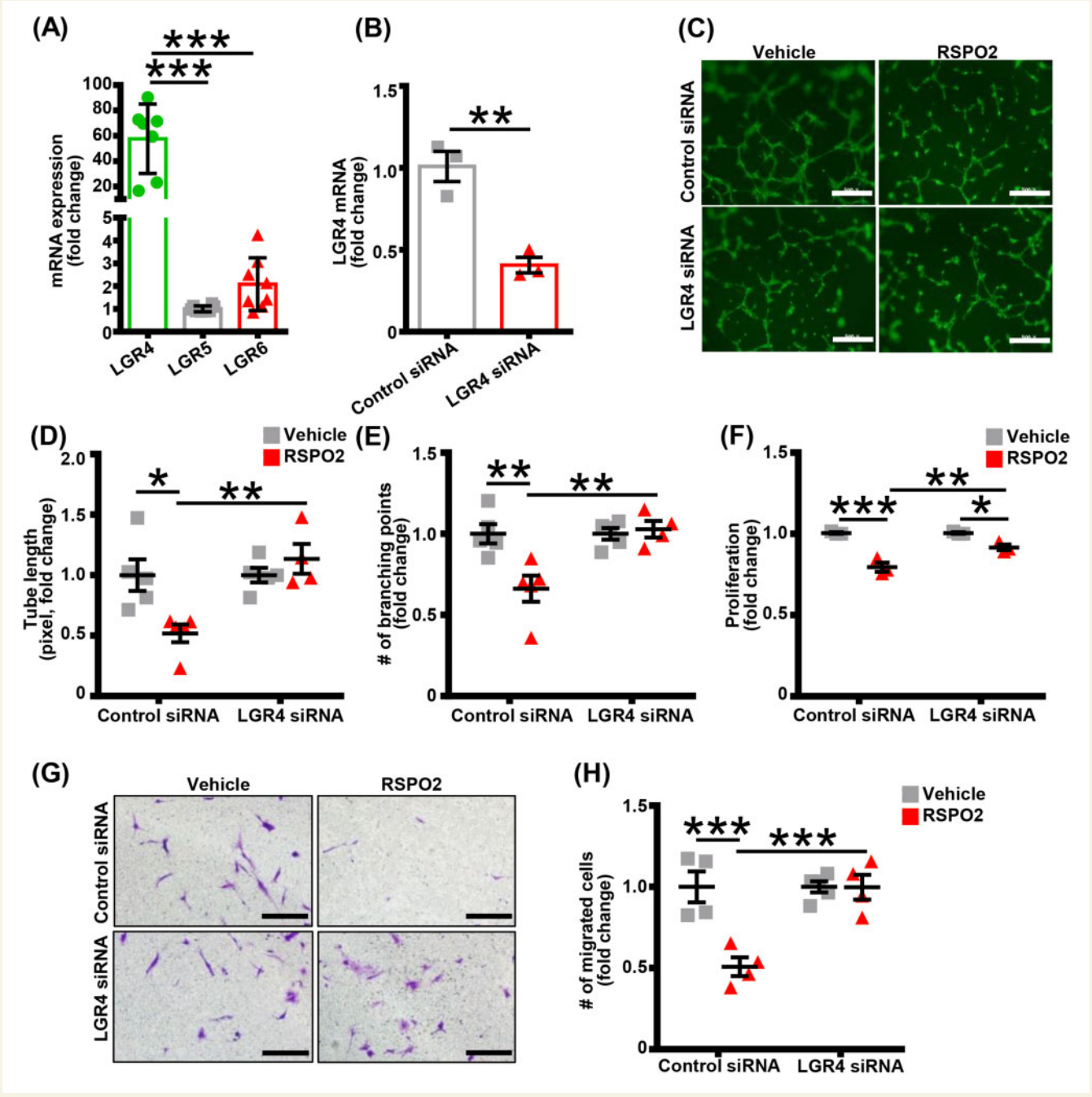

Figure 3 RSPO2 inhibits lymphangiogenesis via LGR4-mediated mechanisms. (*A*) Human LEC were used to extract total RNA and qRT-PCR performed to determine the relative levels of LGR receptors. GAPDH was used as an internal control. Bar graph represents mRNA levels of LGR receptors in comparison to LGR5 (gene with the lowest expression) ($n = 7–8$). (*B*) Control and LGR4 siRNA-treated LEC were utilized to extract RNA and LGR4 levels were quantified using qRT-PCR to confirm successful silencing ($n = 3$). (*C–E*) Control and LGR4-silenced LEC pretreated with vehicle or RSPO2 for 6 h were used for Matrigel tube formation assay as described in *Figure 2E*. Tubes were stained with Alexa Fluor 488-phalloidin and images captured using a Zeiss 780 inverted confocal microscope. Representative photomicrographs are shown (*C*). Scale bar 500 µm. Tube length (*D*) and number of branching points (*E*) were quantified ($n = 4–5$). (*F*) MTT assay was employed to investigate the proliferation of control and LGR4-silenced LEC in response to RSPO2 treatment as described in *Figure 2A*. Data are representative of three independent experiments performed at least in triplicate. (*G*) Control and LGR4-silenced LEC were used to evaluate cell migration as described in *Figure 2C*. Scale bar 200 µm. (*H*) Bar graph represents the number of migrated cells ($n = 4$). Statistical analyses were performed using one-way ANOVA (*A*), two-tailed unpaired *t*-test (*B*), and two-way ANOVA (*D–F* and *H*). Data represent mean ± SEM. $^{*}P < 0.05$, $^{**}P < 0.01$, and $^{***}P < 0.001$. RSPO2, R-spondin 2.

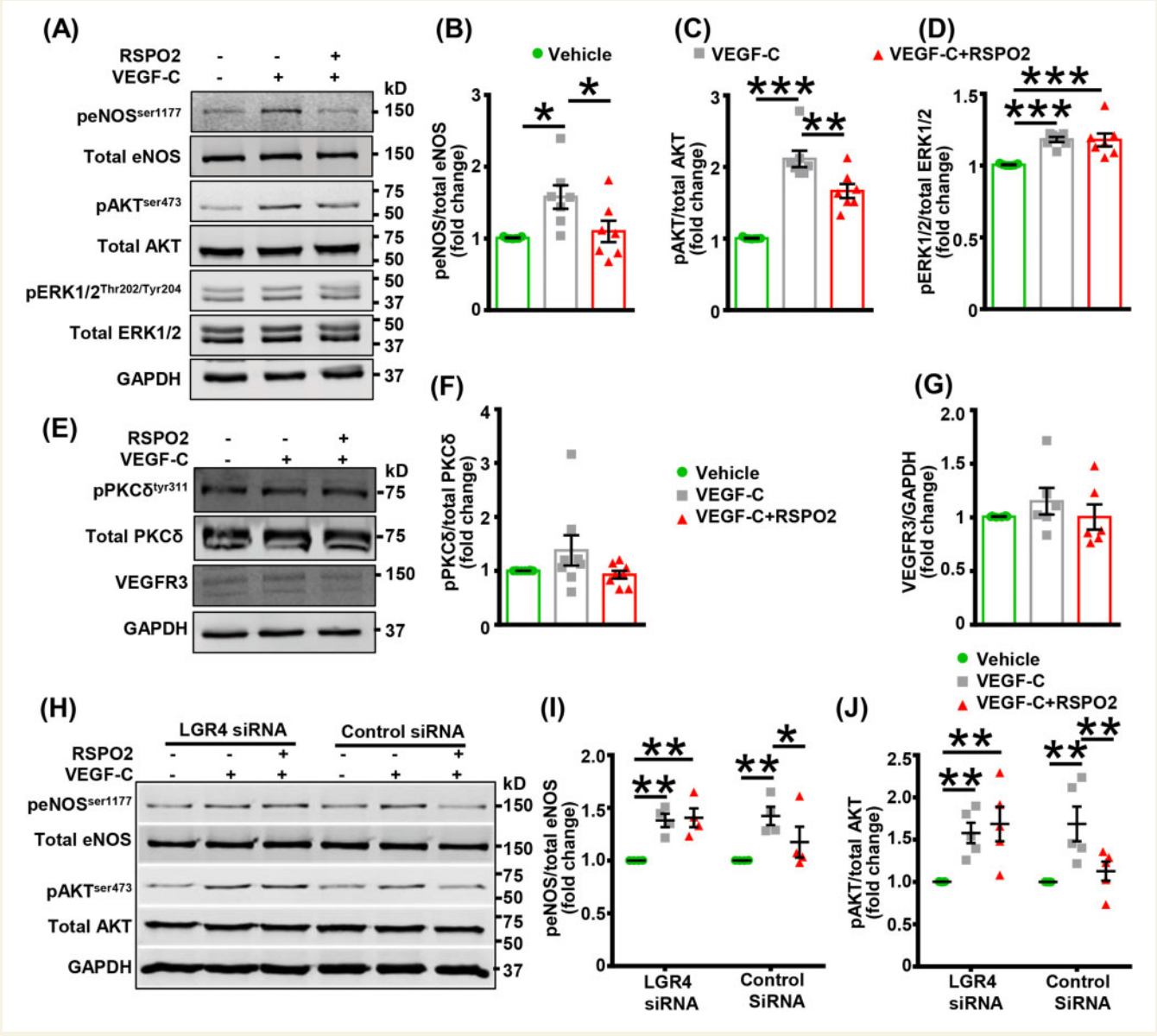

Figure 4 RSPO2 inhibits VEGF-C-stimulated AKT and eNOS activation in LEC. (*A–G*) LEC were serum-starved in 0.5% FBS containing basal media MV2 for 16 h. Then, LEC were pretreated with RSPO2 (6 h), stimulated with VEGF-C for 15 min, and subjected to western blot analysis. (*A* and *E*) Representative western blot images are shown. (*B–D* and *F*) Bar diagrams represent averaged protein levels expressed as a ratio of phospho to total proteins, eNOS (*B*), AKT (*C*), ERK1/2 (*D*), and PKCδ (*F*) ($n = 6–8$). (*G*) Bar diagram represents the mean expression of VEGFR3 normalized with GAPDH ($n = 6$). (*H–J*) Control and LGR4-silenced LEC were used for this experiment. The details of treatment are same as in (*A*). (*H*) Representative western blot images are shown. (*I* and *J*) Bar diagrams represent averaged protein levels expressed as a ratio of phospho to total proteins, eNOS (*I*) ($n = 4$) and AKT (*J*) ($n = 5$). Statistical analyses were performed using one-way ANOVA (*B–D*, *F*, and *G*) and two-way ANOVA (*I* and *J*). Data represent mean ± SEM. $^{*}P < 0.05$, $^{**}P < 0.01$, and $^{***}P < 0.001$. eNOS, endothelial nitric oxide synthase; LEC, lymphatic endothelial cells; RSPO2, R-spondin 2; VEGF, vascular endothelial growth factor.

3.3 RSPO2 suppresses lymphangiogenesis via LGR4-mediated signalling

Three LGR, namely LGR4, LGR5, and LGR6, have been described as high-affinity cell surface receptors for RSPOs.[19,20] To determine the specific LGR receptor(s) involved in RSPO2-mediated inhibition of lymphangiogenesis, we first investigated the relative mRNA levels of LGR4–6 in human LEC using qRT-PCR. The qRT-PCR experiments identified LGR4 as the dominant RSPO2 receptor in LEC (nearly 60 times of LGR5 expression) (*Figure 3A*). The role of LGR4 in RSPO2-induced inhibition of lymphangiogenesis was examined using siRNA-mediated silencing of LGR4 in LEC. The successful silencing of LGR4 in LEC was confirmed by qRT-PCR (*Figure 3B*). As shown in *Figure 3C–H*, LGR4-silencing in LEC significantly attenuated the inhibitory effect of RSPO2 on LEC tube formation (*Figure 3C–E*), proliferation (*Figure 3F*), and migration (*Figure 3G and H*) *in vitro*. Furthermore, inhibition of RSPO2–LGR4 signalling using the LGR4 blocking peptide (LGR4-ECD[21]) abrogated RSPO2-induced

suppression of LEC proliferation compared with control treatment (Supplementary material online, *Figure S4C*). These data demonstrate that LGR4 is required for RSPO2-mediated inhibition of lymphangiogenesis.

3.4 RSPO2 hinders VEGF-C-stimulated AKT and eNOS activation in LEC

VEGF-C stimulates lymphangiogenesis via VEGFR3-mediated activation of AKT, ERK, and eNOS signalling.[9,10] To investigate the mechanism by which RSPO2 inhibits lymphangiogenesis, we treated human LEC with RSPO2 (100 ng/mL, 6 h) followed by incubation with VEGF-C (100 ng/mL) for 15 min and performed western blot experiments to determine activating phosphorylation of eNOS, AKT, and ERK1/2. Cells were stimulated with VEGF-C for 15 min because we observed maximum activation of eNOS, AKT, and ERK1/2 after 15 min of incubation with VEGF-C (data not shown). Our results demonstrated that VEGF-C treatment increased phosphorylation of eNOS (Ser-1177), AKT (Ser-473), and ERK1/2 (Thr-202/Tyr-204) in human LEC (*Figure 4A–D*). Furthermore, RSPO2 treatment significantly reduced VEGF-C-induced phosphorylation of eNOS and AKT, however, no effect on ERK1/2 activation was observed with RSPO2 exposure (*Figure 4A–D*). As the role of PKCδ in VEGF-C/VEGFR3-induced stimulation of lymphangiogenesis has been demonstrated and PKC can activate eNOS and AKT,[39–41] we next investigated PKCδ phosphorylation at Tyr-311 following RSPO2 treatment. As shown in *Figure 4E and F*, VEGF-C exposure did not increase Tyr-311 phosphorylation of PKCδ in LEC and phosphorylation was not affected by RSPO2 pretreatment. Control experiments demonstrate that RSPO2 treatment does not decrease VEGFR3 expression in LEC (*Figure 4E and G*).

Since LGR4 is the major RSPO2 receptor in LEC and LGR4 knockdown inhibited RSPO2's effect on lymphangiogenesis, we next investigated the role of LGR4 in RSPO2-induced suppression of eNOS and AKT activation. Control siRNA-treated and LGR4-silenced cells were used to investigate VEGF-C-stimulated eNOS and AKT phosphorylation following RSPO2 treatment. Notably, the silencing of LGR4 prevented RSPO2-mediated inhibition of eNOS and AKT phosphorylation in LEC (*Figure 4H–J*). In addition, western blot data suggest that RSPO2 did not affect PKCδ activation in control and LGR4-silenced LEC (Supplementary material online, *Figure S4D*). Altogether, these results suggest that RSPO2 inhibits lymphangiogenesis via LGR4-mediated suppression of AKT and eNOS activation.

3.5 Supplementation of NO by SNP inhibits RSPO2's anti-lymphangiogenic activity

As (i) NO is a key mediator of lymphangiogenic activity in VEGF-C-treated cells,[11] (ii) eNOS is the major source of NO in LEC,[11,42] and (iii) we found attenuated VEGF-C-induced eNOS activation in RSPO2-treated cells, we next quantified DAF-FM fluorescence in LEC as a measure of NO bioavailability following RSPO2 treatment. Consistent with increased eNOS phosphorylation (*Figure 4A*), VEGF-C treatment stimulated DAF-FM fluorescence compared with vehicle, and pretreatment of LEC with RSPO2 prevented VEGF-C-stimulated DAF-FM fluorescence (*Figure 5A*). Increased superoxide anion ($O_2^{\bullet-}$) production scavenges NO and stimulation of ROS levels in LEC suppresses lymphangiogenesis.[34] We, therefore, examined whether RSPO2 stimulates ROS production in LEC, leading to decreased NO bioavailability and impaired lymphangiogenesis. Intracellular ROS generation in response to RSPO2 was assessed by measuring H2DCFDA fluorescence using flow cytometry. Flow cytometry data indicated higher ROS levels in LEC treated with RSPO2 compared with vehicle-treated cells (*Figure 5B*). Interestingly, qRT-PCR data demonstrated that Nox4 is the predominant NADPH oxidase (Nox) isoform (*Figure 5C*) in human LEC, followed by Nox1 and Nox5. As H2DCFDA detects various ROS and free radicals ($RO_2^{\bullet}$, $OH^{\bullet}$, $ONOO^{-}$, H_2O_2, etc.) with varying sensitivity and Nox4 primarily generates H_2O_2, we measured H_2O_2 production in RSPO2-treated LEC using Amplex Red fluorescence. As shown in Supplementary material online, *Figure S5*, RSPO2 stimulated H_2O_2 production in human LEC.

To investigate whether pharmacological supplementation of NO or scavenging ROS attenuates RSPO2's inhibitory effect on lymphangiogenesis, LEC were pretreated with the NO donor, SNP, or the cell-permeant superoxide dismutase/catalase mimetic, EUK-134, and cell proliferation following RSPO2 treatment examined. Interestingly, preincubation with SNP prevented RSPO2-induced inhibition of LEC proliferation (*Figure 5D*), however, EUK-134 pretreatment did not alter the inhibitory effect of RSPO2 (*Figure 5E*). Next, we performed a Matrigel tube formation assay using cells pretreated with or without SNP. As shown in *Figure 5F*, VEGF-C + RSPO2 + SNP-treated LEC had tube length and number of branching points similar to VEGF-C-treated LEC, and significantly higher than LEC treated with VEGF-C + RSPO2. Moreover, Matrigel plug experiments were performed to determine the involvement of NO signalling in RSPO2-induced impairment of lymphangiogenesis *in vivo*. Fluorescence microscopy results demonstrated increased LYVE-1 positive staining in VEGF-C + RSPO2 + SNP containing Matrigel plugs compared to VEGF-C + RSPO2 Matrigel plugs (*Figure 5G*). Collectively, these findings indicate that RSPO2 inhibits lymphangiogenesis via impaired NO biogenesis rather than ROS-mediated impairment of NO bioavailability.

3.6 RSPO2 inhibits Wnt-β-catenin signalling in VEGF-C-treated LEC

RSPO2 has been shown to potentiate Wnt signalling in various cell types, including HEK293 cells, osteoblasts, glioblastoma cell lines (U87 and U251), and hepatocytes.[36,43–45] Mechanistically, RSPO2 promotes internalization of the membrane ubiquitinase ZNRF3/RNF43, enabling Wnt-dependent phosphorylation of LDLR-related protein 5/6 (LRP5/6), leading to nuclear translocation of β-catenin and subsequent expression of Wnt target genes.[46] Interestingly, NO production upregulates Wnt-β-catenin signalling in cancer cells and Prox1 has recently been shown to interact with β-catenin to promote LV formation during development.[47,48] These observations prompted us to investigate the effects of RSPO2 on Wnt-β-catenin signalling in LEC. Activation of the Wnt-β-catenin pathway was determined by immunoblotting via assessing the phosphorylation status of LRP6 in HEK293 cells (positive control) and LEC following stimulation with RSPO2. VEGF-C treatment increased LRP6 phosphorylation (Ser-1490) in LEC, which was prevented by pretreatment with RSPO2 (*Figure 6A and B*). Furthermore, as shown in Supplementary material online, *Figure S6*, RSPO2 treatment did not alter phosphorylated LRP6 levels in LEC not exposed to VEGF-C. On the other hand, the levels of phosphorylated LRP6 were remarkably increased in HEK293 cells following RSPO2 treatment (*Figure 6A*). In addition, VEGF-C-induced nuclear translocation of β-catenin in LEC was inhibited by RSPO2 as determined by confocal imaging (*Figure 6C and D*). Next, we performed western blot experiments to examine β-catenin protein levels in nuclear and cytoplasmic fractions of LEC treated with vehicle, VEGF-C, VEGF-C + RSPO2, and RSPO2 alone. As shown in

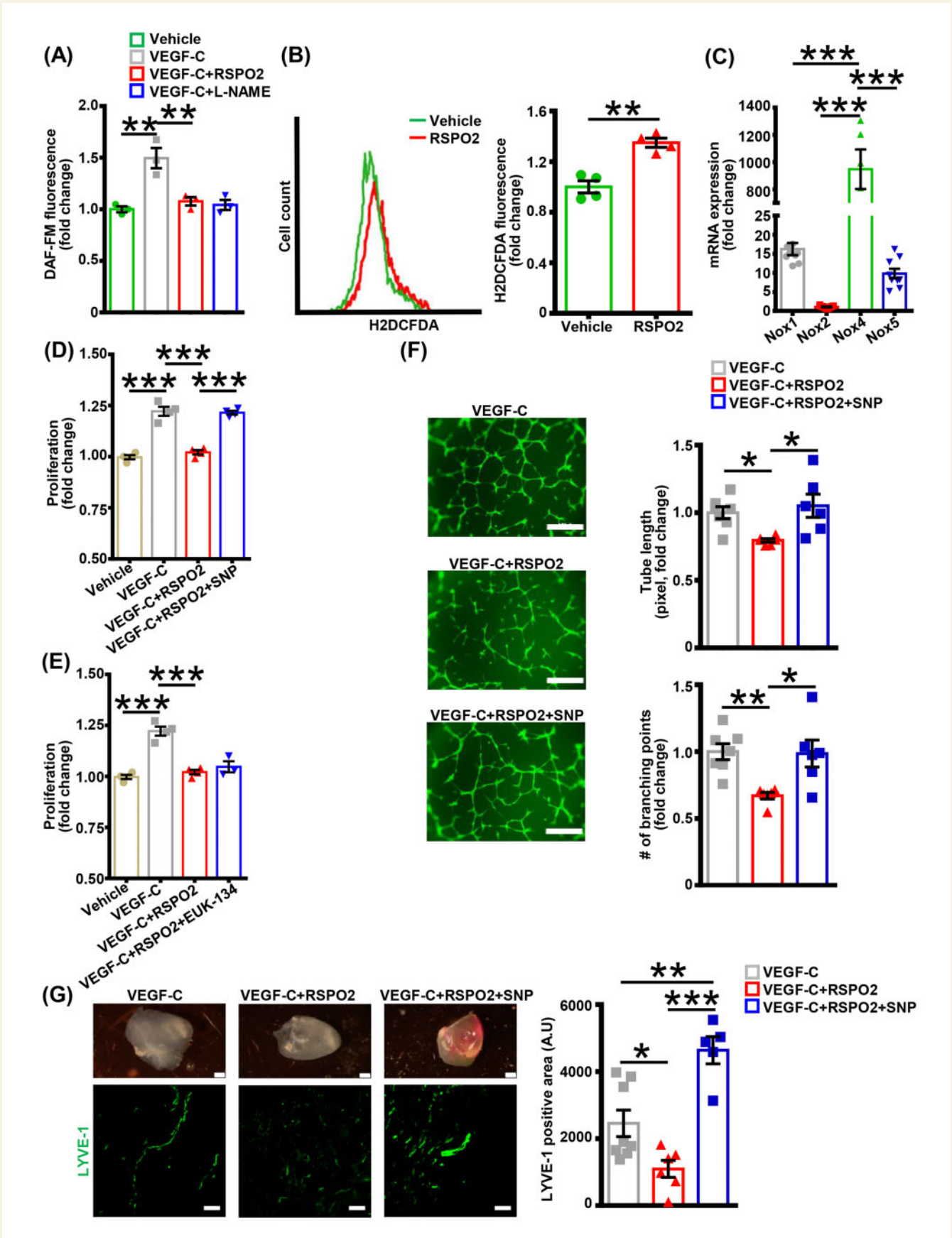

Figure 5 Supplementation of nitric oxide by SNP abrogates RSPO2's anti-lymphangiogenic activity. (*A*) Vehicle or RSPO2-pretreated LEC (6 h) were stimulated with VEGF-C for 1 h, washed, incubated with DAF-FM diacetate, and fluorescence determined (excitation/emission 495/515 nm). L-NAME pretreated cells were used as negative controls. Data are representative of three independent experiments performed in triplicate. (*B*) LEC were treated with vehicle or RSPO2 for 30 min, incubated with H2DCFDA and fluorescence analysed using flow cytometry. Representative histograms showing

Figure 6E, VEGF-C stimulation significantly increased β-catenin expression in the nucleus compared with vehicle treatment. VEGF-C-induced nuclear β-catenin expression was inhibited by pretreatment with RSPO2. Then, we speculated that the inhibitory effects of RSPO2 on β-catenin signalling may be mediated by impaired NO production and provide a possible explanation for its growth-suppressive potential in LEC. L-NAME was utilized to investigate the role of NO signalling in β-catenin translocation to the nucleus. Pretreatment of LEC with L-NAME inhibited VEGF-C-stimulated nuclear β-catenin expression indicating the role of NO signalling in β-catenin translocation to the nucleus (*Figure 6E*). In addition, we did not observe any differences in nuclear β-catenin levels in LEC treated with VEGF-C + RSPO2 and VEGF-C + RSPO2 + L-NAME, suggesting that RSPO2-induced inhibition of nuclear β-catenin translocation is mediated by impaired NO signalling. Altogether, these results suggest that RSPO2 attenuates Wnt-β-catenin signal transduction in LEC via decreasing NO-mediated nuclear translocation of β-catenin.

3.7 Blockade of RSPO2–LGR4 signalling attenuates atherosclerosis

The role of RSPO2–LGR4 signalling in the regulation of arterial LV density, arterial cholesterol removal, and pathogenesis of atherosclerosis has not been previously investigated. We first isolated mouse primary lung LEC to examine whether LGR4 is the predominant RSPO2 receptor in mouse LEC. Immunostaining was used to confirm the co-expression of LEC markers LYVE-1 and VEGFR3 and determine the purity of isolated murine LEC (Supplementary material online, *Figure S7A*). Similar to human LEC, qRT-PCR data showed that LGR4 is the major RSPO2 receptor in mouse LEC (Supplementary material online, *Figure S7B*). To study the role of RSPO2–LGR4 signalling in the development of atherosclerotic lesions, we utilized a modified partial LCA ligation model, which creates oscillatory flow in the artery and promotes atherosclerosis. After partial ligation of LCA branches in $ApoE^{-/-}$ mice, the efferent LV around the LCA were disconnected from the periarterial tissue and pluronic gel containing LGR4-blocking mouse LGR4/Gpr48 Fc chimeric protein (LGR4-ECD[21]) or mouse IgG_{2a} (control) was applied periadventitially (*Figure 7A*).[7,49] The N-terminal ECD of LGR4 has been recognized as the binding site for the LGR4 ligands RSPOs[20] and LGR4-ECD has been shown to inhibit LGR4 signalling both *in vitro* and *in vivo*.[21] Control experiments demonstrate that LGR4-ECD blocks RSPO2's inhibitory effects on LEC proliferation *in vitro* (Supplementary material online, *Figure S4C*). After 3 weeks of Western diet, fasting blood glucose, plasma total cholesterol, body weight, and body composition were determined. As shown in *Figure 7B and C* and Supplementary material online, *Figure S8A and B*, there were no differences in plasma total cholesterol, body weight, fat and lean mass, and fasting blood glucose between LGR4-ECD-treated and control mice. Interestingly, the periadventitial application of LGR4-ECD attenuated atherosclerotic lesion formation in the LCA compared with control treatment (*Figure 7D and E*). Lipid deposition was remarkably reduced in the proximal (1–300 μm, *Figure 7E and G*) and middle (1800–2100 μm, *Figure 7E and H*) LCA segments of mice treated with LGR4-ECD perivascularly, however, no differences in lipid deposition were observed in the distal LCA regions immediately adjacent to the partial ligation (3600–3900 μm, *Figure 7E and I*). Representative ORO and H&E staining, and quantified neointimal area are shown in *Figure 7E, J, and K*, respectively. Furthermore, there were no differences in arterial RSPO2 protein levels between LGR4-ECD-treated and control groups (data not shown). Consistent with reduced atherosclerotic lesion formation, CD68 staining was decreased in the LCA of LGR4-ECD-treated mice indicating reduced macrophage accumulation following pharmacological blockade of LGR4 activation (*Figure 7J and M*). Finally, Masson's trichrome staining for collagen was increased in LCA sections of LGR4-ECD-treated mice compared with control animals (*Figure 7J and L*). Taken together, these results suggest that blockade of RSPO-mediated LGR4 activation protects hypercholesterolemic mice from the development of atherosclerosis.

3.8 Inhibition of LGR4-mediated signalling increases lymphatic vessel density in hypercholesterolemic mice and promotes arterial efflux of cholesterol

To investigate whether perivascular application of LGR4-ECD increases LV density in the adventitial layer and improves lymphatic drainage of arterial cholesterol in $ApoE^{-/-}$ mice, LYVE-1 positive area in the LCA and

Figure 5 Continued

H2DCFDA fluorescence are shown. The *X*-axis is logarithmic. Bar diagram indicates mean fluorescence intensity in different groups ($n = 4$). (*C*) Human LEC were used to extract RNA and qRT-PCR was performed to determine levels of Nox1, Nox2, Nox4, and Nox5 expression. GAPDH was used as an internal control. Bar graph represents mRNA levels of different Nox isoforms in comparison to Nox2 (gene with the lowest expression). Data are representative of three independent experiments performed in triplicate. (*D* and *E*) LEC were pretreated with vehicle, SNP (1 μM, *D*) or EUK-134 (100 nM, *E*) for 30 min, then incubated with RSPO2 (6 h), stimulated with VEGF-C for 48 h and proliferation investigated using MTT assay. Data are representative of three to four independent experiments performed at least in triplicate. (*F*) LEC pretreated with vehicle or SNP (30 min) were incubated with RSPO2 for 6 h, trypsinized, and seeded in wells of Matrigel-coated plate in basal medium containing VEGF-C, VEGF-C + RSPO2, and VEGF-C + RSPO2 + SNP, and tube formation determined (6 h). Representative photomicrographs are shown. Scale bar 200 μm. Bar diagrams indicate tube length and number of branching points ($n = 6–7$). (*G*) Matrigel plugs mixed with VEGF-C, VEGF-C + RSPO2, or VEGF-C + RSPO2 + SNP were implanted subcutaneously in wild-type mice. Plugs were isolated after 2 weeks, sectioned and immunostained for LYVE-1. Bar diagram shows quantitative analysis of LYVE-1 positive area in implanted Matrigel plugs ($n = 5–8$). Statistical analyses were performed using one-way ANOVA (*A* and *C–G*) and two-tailed unpaired *t*-test (*B*). Data represent mean ± SEM. $^{*}P < 0.05$, $^{**}P < 0.01$, and $^{***}P < 0.001$. L-NAME, L-N^{G}-Nitro arginine methyl ester; LEC, lymphatic endothelial cells; LYVE-1, lymphatic vessel endothelial hyaluronan receptor-1; RSPO2, R-spondin 2; SNP, sodium nitroprusside; VEGF, vascular endothelial growth factor.

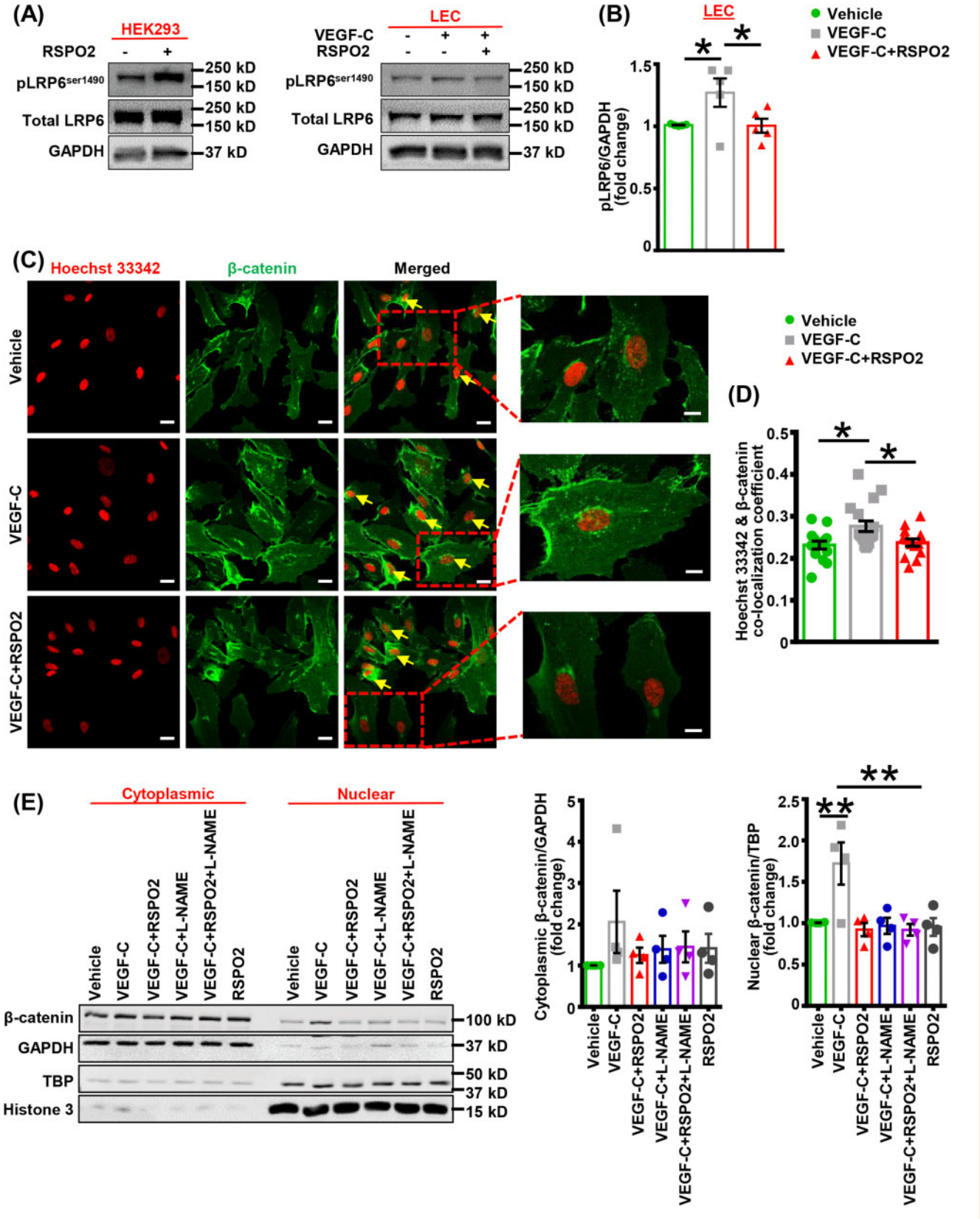

Figure 6 RSPO2 impairs Wnt-β-catenin signalling in VEGF-C-stimulated LEC. (*A*) HEK293 were treated with RSPO2 for 6 h and subjected to western blot analysis for LRP6 phosphorylation (left panel). LEC were serum-starved in 0.5% FBS containing basal media MV2 for 16 h. Then, LEC were pretreated with RSPO2 (6 h), stimulated with VEGF-C for 15 min, and subjected to western blot (right panel). (*B*) Bar diagram represents mean protein levels expressed as a ratio of phospho to total protein ($n = 5$). (*C*) LEC grown on coverslips were pretreated with vehicle or RSPO2 (6 h) and stimulated with VEGF-C for 15 min. Cells were fixed and immunostained for β-catenin (green). Nuclei were counterstained with Hoechst 33342 (red). At least five images of randomly

LDL levels in plaque (i.e. LCA)-draining deep cervical LN, skin-draining inguinal LN (negative control), liver, spleen, and LCA tissue were quantified. As shown in *Figure 7N and O*, LGR4-ECD treatment increased LYVE-1 positive staining compared with control treatment indicating the development of a more extensive network of LV in the arterial wall following pharmacological blockade of LGR4. Next, LGR4-ECD-treated and control mice were injected retro-orbitally with fluorescently (DiI)-labelled LDL (70 μg/30 g body weight) and DiI fluorescence was determined in deep cervical LN, inguinal LN, liver, spleen, and LCA 24 h after injection. DiI fluorescence in plasma was quantified 4, 8, and 24 h after injection. We used this model as a previous study reported the accumulation of DiI-LDL in atherosclerotic lesions following retro-orbital administration.[50] Arterial cholesterol efflux to the deep cervical LN immediately adjacent to LCA on the left side was quantified, as this is the most proximal LN to the carotid artery bifurcation (Supplementary material online, *Figure S3A*). Confirming the functional role of the deep cervical LN in arterial cholesterol efflux, our experiments demonstrated increased LCA atherosclerosis following surgical removal of this LN compared with sham-operated controls (Supplementary material online, *Figure S3B–D*). As shown in *Figure 7P*, no significant differences in DiI fluorescence (excitation: 549 nm and emission: 565 nm) were observed in the plasma of control and LGR4-ECD-treated mice 4, 8, or 24 h post-DiI-LDL injection. DiI fluorescence in inguinal LN not associated with arterial lesions was very low (control—2228.2 ± 586.05 vs. LGR4-ECD—2382.4 ± 662.9) (*Figure 7R*) compared to lesion-draining LN (control—19 493.4 ± 3500.9 vs. LGR4-ECD—52 634.0 ± 4372.7), demonstrating that DiI-LDL enters deep cervical LN directly from the LCA wall and not from the circulation. Our results also indicated that levels of DiI fluorescence were significantly higher in lesion-draining deep cervical LN of mice treated with LGR4-ECD compared with controls, indicating increased removal of DiI-LDL from the arterial wall following pharmacological blockade of periadventitial RSPO2–LGR4 signalling (*Figure 7R*). Consistent with this statement immunofluorescence analysis of the LCA wall demonstrated attenuated DiI fluorescence in LGR4-ECD-treated mice compared with control animals (*Figure 7Q*). As the majority of DiI-LDL enters the liver and spleen directly from the circulation, we did not observe differences in DiI fluorescence between LGR4-ECD-treated and control animals (Supplementary material online, *Figure S8C and D*). Taken together, these findings suggest that pharmacological blockade of LGR4 activation increases LV density, leading to increased cholesterol efflux from atherosclerotic arteries to the lymphatic network and attenuated atherosclerosis development.

4. Discussion

The lymphatic vasculature represents the primary route of cholesterol removal from atherosclerotic vessels via RCT.[6] Enhancing LV density/function has beneficial effects in various pathological conditions, including hypertension, obesity, diabetes, atherosclerosis, oedema formation, and renal fibrosis.[12,51–54] In the present study, we evaluated the role of RSPO2 in the regulation of lymphangiogenesis and development of atherosclerosis. Herein, using *in vitro* and *in vivo* approaches, we report novel discoveries demonstrating that (i) human and mouse atherosclerotic arteries have increased expression of matricellular protein RSPO2 in the adventitial layer, where LV are primarily localized,[4] (ii) RSPO2 inhibits lymphangiogenesis both *in vitro* and *in vivo*, (iii) RSPO2 reduces VEGF-C/VEGFR3-mediated eNOS activation and inhibits canonical Wnt-β-catenin signalling in LEC, and (iv) perivascular application of RSPO2's decoy receptor increases arterial LV density in hypercholesterolemic mice, promotes arterial cholesterol removal and attenuates atherosclerosis. These findings are expected to spur broader research into matrix regulation of lymphangiogenesis, lymph-mediated lipid transport, and regulation of inflammation via removal of interstitial fluid, immune cells, and cytokines from peripheral tissue. On a more translational level, these findings may have broad implications for various pathological conditions associated with impaired lymphatic function and development of new interventions improving RCT, attenuating atherosclerosis development and promoting lesion regression.

Recent studies have identified shared genetic and molecular factors central to cancer development and pathogenesis of CVD and tested whether therapeutic applications commonly used for the treatment of cancer can be applied to the prevention of atherosclerosis and vice versa.[55] Although the Wnt signalling pathway is emerging as a pathological link between CVD and cancer,[55] the role of Wnt regulatory RSPOs in atherosclerosis has not been previously investigated. In mammals, four types of RSPO (RSPO1–4) are expressed and bind any of the three LGR (4–6) receptors.[56] RSPO play significantly different functions irrespective of similar cell surface receptors. To address the role of RSPO in atherosclerosis, we first investigated the expression of RSPO1, 2, and 3 in human atherosclerotic arteries and non-atherosclerotic control tissue. Western blot data revealed increased expression of RSPO2 in atherosclerotic arteries compared to non-atherosclerotic vascular tissue, however, RSPO1 levels were significantly lower in the atherosclerotic region compared with non-atherosclerotic arterial segments. Furthermore, to dissect the role of RSPO2 in atherosclerosis, we investigated the localization and expression of RSPO2 in human and murine atherosclerotic and plaque-free arteries. Western blot and immunostaining data demonstrated increased RSPO2 expression in the adventitial, medial, and neointimal layers of atherosclerotic arteries. The qRT-PCR data revealed elevated RSPO2 mRNA levels in human AoAF compared to aortic SMC. A previous study has also shown fibroblasts (lung) as the major producer of RSPO2.[24] Nonetheless, relative expression of RSPO2 in macrophages, adventitial fibroblasts, and arterial SMC exposed to pathological mediators relevant to atherosclerosis (e.g. ROS, inflammatory cytokines, oxidized lipids, etc.) might be different compared with untreated cells used

Figure 6 Continued

chosen microscopic fields were captured. Representative images are shown. Scale bar 20 μm. Enlarged images; scale bar 10 μm. (*D*) Bar graph represents the mean co-localization coefficient for Hoechst 33342 and β-catenin ($n = 14–17$). (*E*) LEC were treated as indicated, nuclear-cytoplasmic fractionation conducted, and western blot experiments performed using nuclear and cytoplasmic fractions of LEC. GAPDH was used as cytoplasmic control. TBP and histone 3 were used to determine the purity of nuclear preparations. Bar diagram represents mean β-catenin levels in cytoplasmic and nuclear fractions ($n = 4$). Statistical analyses were performed using one-way ANOVA (*B*, *D*, and *E*). Data are presented as mean ± SEM. $^*P < 0.05$ and $^{**}P < 0.01$. L-NAME, L-N^G-Nitro arginine methyl ester; LEC, lymphatic endothelial cells; RSPO2, R-spondin 2; TBP, TATA-binding protein; VEGF, vascular endothelial growth factor.

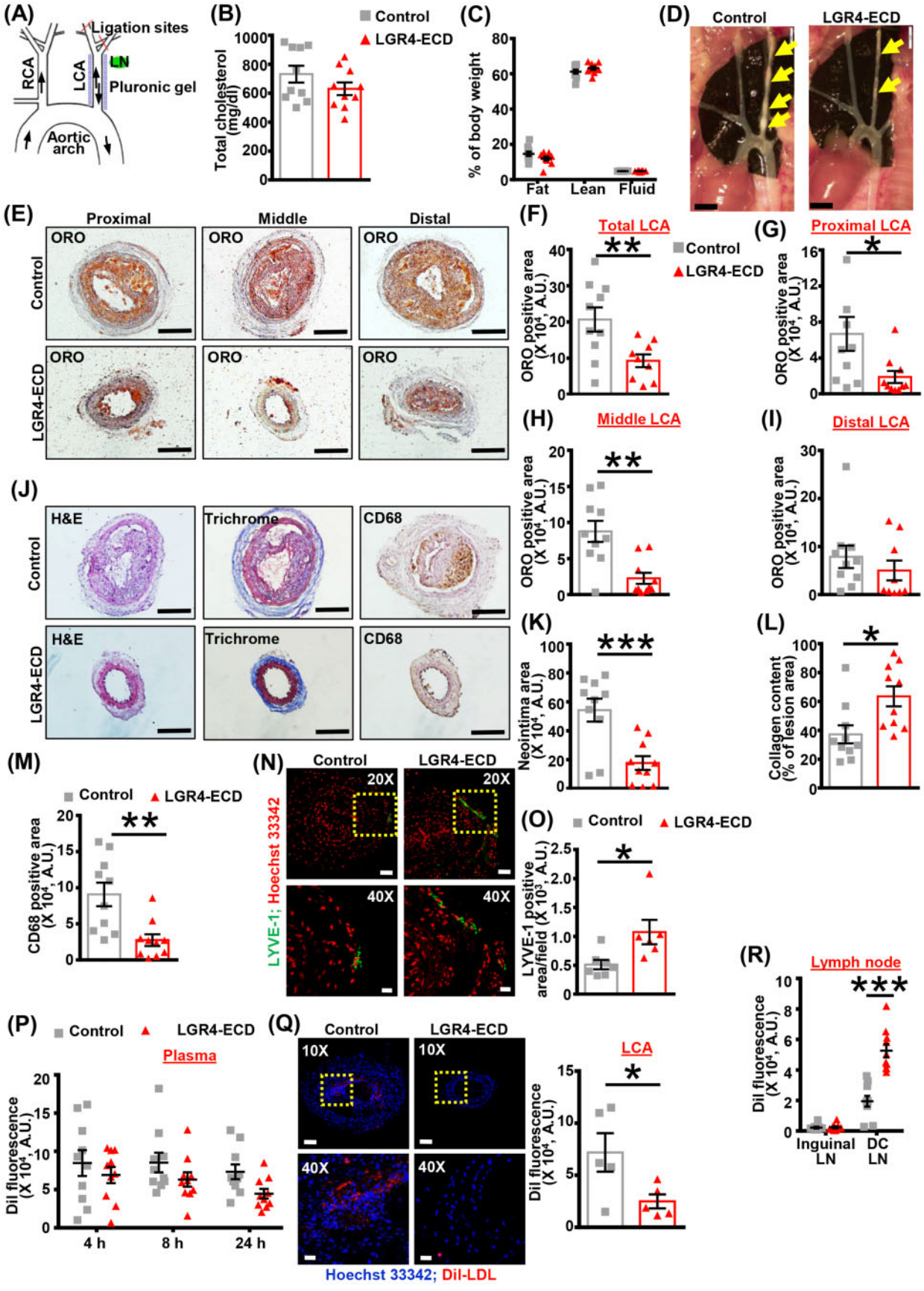

Figure 7 Blockade of periadventitial RSPO2–LGR4 signalling increases the density of lymphatic vessels in the arterial wall and attenuates atherosclerosis development. (*A*) Scheme of partial ligation of LCA, the position of LCA-draining deep cervical LN (green), and periarterial application of control/LGR4-ECD containing pluronic gel (blue). (*B* and *C*) Male ApoE$^{-/-}$ mice underwent partial LCA ligation, disruption of efferent LV, and application of control or

in the present study. Our experiments, consistent with previous reports,[4,6] identified LV mainly in the adventitial layer of atherosclerotic arteries. The present study demonstrated that surgical removal of deep cervical LN adjacent to the LCA promotes atherosclerosis development in ApoE$^{-/-}$ mice following partial LCA ligation. These results are in line with previous observations demonstrating that surgical (transplantation of ApoE$^{-/-}$ aorta loaded with [^{2}H]$_6$-labelled cholesterol to ApoE$^{-/-}$ recipient mice treated with a control/VEGFR3-blocking antibody and ApoE adenoviral vector to inhibit LV formation) and genetic [Chy mice (haploinsufficient VEGFR3 mutant mice) and soluble VEGFR3 overexpressing mice on LDLR$^{-/-}$/ApoB$^{100/100}$] disruption of lymphatic flow impairs RCT and promotes atherosclerosis development.[6,57] Activation of VEGF-C/VEGFR3 signalling stimulates proliferation and migration of LEC and formation of LV *in vitro* and *in vivo*.[58,59] Despite increased VEGF-C levels in atherosclerotic arteries, adventitial LV density and related lymphatic cholesterol efflux are insufficient to promote plaque regression in atherosclerotic vessels.[5] Although these results suggest that VEGF-C signalling is inhibited in atherosclerotic vessels, the precise mechanisms remain unknown.[60] As RSPO2 levels are elevated in the adventitial layer of atherosclerotic arteries where LV regress during the development of atherosclerosis, we examined the effects of RSPO2 on LEC proliferation, migration, and tube formation. Our results indicated that RSPO2-pretreated LEC exhibited reduced proliferation, migration, and tube formation compared with control cells. In addition, *in vivo* Matrigel plug assay confirmed the anti-lymphangiogenic effects of RSPO2.

Next, we investigated the molecular mechanisms by which RSPO2 suppresses lymphangiogenesis. Quantitative RT-PCR and siRNA-mediated silencing experiments demonstrated LGR4 as the major RSPO2 receptor in LEC and that repression of lymphangiogenesis by RSPO2 is LGR4-dependent. Consistent with siRNA-mediated knockdown data, RSPO2's anti-lymphangiogenic effect was inhibited by the pharmacological blockade of LGR4 activation using LGR4-ECD. VEGFR3 upon activation by VEGF-C, undergoes phosphorylation, leading to activation of downstream signalling involving PKC, AKT, ERK1/2, and eNOS phosphorylation.[41,61] We observed reduced VEGF-C-induced AKT and eNOS activation in RSPO2-challenged LEC in comparison to VEGF-C-treated cells. The silencing of LGR4 in LEC inhibited RSPO2's effect on AKT and eNOS activation. NO signalling is critical for lymphangiogenesis and maintenance of lymphatic function.[12] In addition, increased ROS generation reduces NO bioavailability and inhibits lymphangiogenesis.[34] RSPO2 stimulates ROS generation in LEC and previous studies indicated increased ROS levels in patients with chronic lymphedema.[62] Despite these results, our studies indicate that impaired NO biogenesis rather than ROS-mediated impairment of NO bioavailability or redox mechanisms are responsible for RSPO2-induced inhibition of lymphangiogenesis. Indeed, we demonstrated that exogenous supply of NO using the NO donor SNP, but not treatment with a cell-permeant antioxidant, abolished inhibitory effects of RSPO2 on lymphangiogenesis. These results are consistent with findings that NO donors (DETA NONOate and Glyco-SNAP-2) induce LEC proliferation in a dose-dependent manner and inhibition of eNOS impedes lymphangiogenesis.[11] Taken together, these findings may have important implications in disease conditions associated with lymphatic regression and impaired drainage of interstitial fluid despite elevated or normal levels of VEGF-C.

Wnt-β-catenin signalling is critical for LV formation during embryonic development.[48] As RSPO2 is an established agonist of β-catenin signalling in various cell types,[36,43–45] we next investigated activation of the Wnt-β-catenin pathway in LEC following RSPO2 treatment. Interestingly, western blot data showed reduced VEGF-C-induced LRP6 phosphorylation in RSPO2-treated LEC, indicating impaired β-catenin signalling. Control experiments performed simultaneously demonstrated that RSPO2 stimulates LRP6 phosphorylation in HEK293 cells, but not in LEC. These results suggest cell-specific effects of RSPO2 treatment on Wnt signalling and are line with a previous report in colorectal cancer cells.[36] Furthermore, our study indicated a functional association between VEGF-C-VEGFR3-NO and Wnt-β-catenin signalling pathways. Warboys *et al.*[63] suggested a bidirectional cross-talk and regulation between the NO-cyclic guanosine-3′,5′-monophosphate and β-catenin pathways. In addition, another

Figure 7 Continued

LGR4-ECD pluronic gel. Mice were fed a Western diet for 3 weeks post-surgery. Total plasma cholesterol levels (*B*), body fat, lean mass, and fluid content (*C*) were analysed ($n = 10$ mice). (*D*) Representative *in situ* images of atherosclerotic plaques (yellow arrows) in the LCA of ApoE$^{-/-}$ mice treated with control or LGR-ECD are shown. (*E*) The isolated LCAs were divided into proximal (1–300 μm), middle (1800–2100 μm), and distal (3600–3900 μm) regions based on their distance from the outer curvature of aortic arch. Representative images of ORO staining are shown. Scale bar: 200 μm. (*F–I*) Bar graphs show quantified ORO positive area in the entire LCA (*F*), proximal LCA (*G*), middle LCA (*H*), and distal LCA (*I*) of control and LGR4-ECD-treated mice ($n = 9$–10 mice; 4 sections/mice). (*J*) Representative images of H&E (neointima), Masson's trichrome, and CD68 staining performed on LCA sections. Scale bar: 200 μm. (*K–M*) Bar diagrams represent quantified neointimal area (*K*), collagen content (*L*), and CD68 positive area (*M*) in the LCA of control and LGR4-ECD-treated mice ($n = 10$ mice; 4 sections/mice). (*N*) Immunofluorescent staining for LYVE-1 (green) was performed on LCA sections of both groups. Nuclei were counterstained with Hoechst 33342 (red). Representative images are shown (upper panels, 20×, scale bar 50 μm). Enlarged images of insets are also shown (lower panels, 40×, scale bar 20 μm). (*O*) Bar graph represents LYVE-1 positive area/field in control and LGR4-ECD segments of LCA ($n = 6$–7 mice). (*P*) Dil fluorescence in plasma of mice 4, 8, and 24 h after Dil-LDL injection ($n = 10$ mice). (*Q*) Representative fluorescent images showing Dil fluorescence in the LCA sections of control and LGR4-ECD-treated mice 24 h after Dil-LDL injection. Dil (red) and Hoechst 33342 (blue). Enlarged images of insets are also shown (upper panels, 10×, scale bar 100 μm; lower panels, 40×, scale bar 20 μm). Bar graph represents mean Dil fluorescence ($n = 5$ mice; 4 sections/mice). (*R*) Quantified data showing Dil fluorescence in skin-draining inguinal LN and LCA-draining deep cervical LN as a measure of LDL efflux from atherosclerotic LCA via lymphatic vessels 24 h after Dil-LDL injection ($n = 10$ mice). Statistical analyses were performed using a two-tailed unpaired *t*-test (*B*, *F–I*, *K–M*, *O*, and *Q*) and two-way ANOVA (*C*, *P*, and *R*). Data are presented as mean ± SEM. $^{*}P < 0.05$, $^{**}P < 0.01$, and $^{***}P < 0.001$. ECD, extracellular domain; H&E, haematoxylin and eosin; LCA, left carotid artery; LN, lymph node; LYVE-1, lymphatic vessel endothelial hyaluronan receptor-1; ORO, Oil Red O; RCA, right carotid artery.

study identified NO as a regulator of canonical Wnt-β-catenin signalling.[64] Our findings demonstrated that RSPO2 treatment reduces the nuclear translocation of β-catenin in LEC via NO-mediated pathways. We speculate that attenuated Wnt-β-catenin signalling may lead to reduced expression of FOXC2 and GATA2 in LEC, which are necessary for LV formation.[48] As RSPO2 deficiency in mice ($Rspo2^{-/-}$) is postnatally lethal,[65] we did not perform genetic studies to evaluate the role of RSPO2 in atherosclerosis. Moreover, no prior studies have investigated lymphatic function or lymphangiogenesis in $Rspo2^{-/-}$ embryos or postnatally, to examine RSPO2's role in LV formation during development. Future studies using LEC-specific LGR4 knockout mice are expected to provide important information on RSPO-mediated LGR4 activation in the regulation of lymphangiogenesis.[66]

Prompted by our findings that human and mouse atherosclerotic plaques have increased RSPO2 expression and RSPO2 attenuates lymphangiogenesis via LGR4-dependent mechanisms, we determined whether blockade of RSPO-mediated LGR4 activation protects mice from atherosclerosis. After partial ligation of LCA branches in $ApoE^{-/-}$ mice, we surgically disconnected the periadventitial lymphatic network from the LCA-draining LN and perivascularly applied pluronic gel to inhibit LGR4 signalling in the adventitial layer. LGR4-ECD treatment enhanced LYVE-1 positive staining in the adventitia, increased arterial cholesterol efflux to LCA-draining LN, but not to skin-draining inguinal LN, and attenuated atherosclerotic lesion area. Consistently, LCA of LGR4-ECD-treated mice had attenuated DiI-LDL levels compared with controls. Furthermore, atherosclerotic lesions in LGR4-ECD-treated mice had lower macrophage accumulation and higher collagen content, which are hallmarks of stable plaques.[67] These data suggest the therapeutic potential of targeted LGR4 inhibition in the treatment of atherosclerosis. Nonetheless, whether LGR4 blockade-induced protection against atherosclerosis exclusively through lymphatics remains to be determined. For example, it is possible that the periarterial blockade of LGR4 signalling regulates the density or structure of vasa vasorum and inhibits the infiltration of inflammatory cells into the arterial wall. Therefore, future studies investigating LV density/function and atherosclerosis in mice with LEC-specific deletion of LGR4 are required. All four RSPO vary in their functions regardless of their binding affinities to similar cell surface receptors. However, it remains to be investigated whether an RSPO protein can regulate the expression of other RSPO and affect downstream signalling.

In summary, the present study suggests that the matrix protein RSPO2 limits LV formation via LGR4-dependent mechanisms, and consequently attenuates lymphatic drainage of LDL cholesterol from the arterial wall, leading to atherosclerosis development. These findings indicate that inhibition of anti-lymphangiogenic signalling may be a potential therapeutic strategy to improve the lymphatic drainage of lipoproteins, promote resolution of inflammation via removal of inflammatory cytokines and immune cells from the inflamed area, and restore tissue homeostasis. However, in cancerous settings, inhibition of anti-lymphangiogenic pathways should be performed cautiously and with local treatment so that there is no tumour progression and metastasis due to a generalized increase in lymphangiogenesis.

Data availability

The data relating to this article are available in the article itself or in its Supplementary material online.

Supplementary material

Supplementary material is available at *Cardiovascular Research* online.

Authors' contributions

B.S. and G.C. designed the study; B.S. performed most of the experiments, analysed data, and wrote the manuscript. H.-P.L. performed left carotid artery ligation in mice. A.C. helped with experiments and data analysis. W.A., M.C.-S., and P.G. assisted in data analysis. J.W. provided non-atherosclerotic and atherosclerotic human arterial tissue. B.K.S. and G.C. provided feedback on experiments, reviewed, and edited the manuscript.

Acknowledgements

We are grateful to David Adams, MBIE, CFSP, and David Johnson, Department of Cellular Biology & Anatomy, Augusta University for providing us human cadaveric tissue. We are also thankful to David Stepp, Yuqing Huo, and Muhammad Ashraf, Augusta University, for allowing us to use their NMR machine, phase-contrast microscope, and cryostat, respectively.

Conflict of interest: none declared.

Funding

This work was supported by the National Institutes of Health [R01HL139562, and R00HL114648 awarded to G.C., and K99HL146954 given to B.S.] and American Heart Association Postdoctoral Fellowship [17POST33661254 given to B.S.].

References

1. Arnett DK, Blumenthal RS, Albert MA, Buroker AB, Goldberger ZD, Hahn EJ, Himmelfarb CD, Khera A, Lloyd-Jones D, McEvoy JW, Michos ED, Miedema MD, Munoz D, Smith SC Jr, Virani SS, Williams KA Sr, Yeboah J, Ziaeian B. 2019 ACC/AHA Guideline on the primary prevention of cardiovascular disease: a report of the American College of Cardiology/American Heart Association Task Force on clinical practice guidelines. *Circulation* 2019;**140**:e596–e646.
2. Fogelstrand P, Boren J. Retention of atherogenic lipoproteins in the artery wall and its role in atherogenesis. *Nutr Metab Cardiovasc Dis* 2012;**22**:1–7.
3. Csanyi G, Singla B. Arterial lymphatics in atherosclerosis: old questions, new insights, and remaining challenges. *J Clin Med* 2019;**8**:495.
4. Drozdz K, Janczak D, Dziegiel P, Podhorska M, Patrzalek D, Ziolkowski P, Andrzejak R, Szuba A. Adventitial lymphatics of internal carotid artery in healthy and atherosclerotic vessels. *Folia Histochem Cytobiol* 2008;**46**:433–436.
5. Taher M, Nakao S, Zandi S, Melhorn MI, Hayes KC, Hafezi-Moghadam A. Phenotypic transformation of intimal and adventitial lymphatics in atherosclerosis: a regulatory role for soluble VEGF receptor 2. *FASEB J* 2016;**30**:2490–2499.
6. Martel C, Li W, Fulp B, Platt AM, Gautier EL, Westerterp M, Bittman R, Tall AR, Chen SH, Thomas MJ, Kreisel D, Swartz MA, Sorci-Thomas MG, Randolph GJ. Lymphatic vasculature mediates macrophage reverse cholesterol transport in mice. *J Clin Invest* 2013;**123**:1571–1579.
7. Rademakers T, van der Vorst EP, Daissormont IT, Otten JJ, Theodorou K, Theelen TL, Gijbels M, Anisimov A, Nurmi H, Lindeman JH, Schober A, Heeneman S, Alitalo K, Biessen EA. Adventitial lymphatic capillary expansion impacts on plaque T cell accumulation in atherosclerosis. *Sci Rep* 2017;**7**:45263.
8. Kutkut I, Meens MJ, McKee TA, Bochaton-Piallat ML, Kwak BR. Lymphatic vessels: an emerging actor in atherosclerotic plaque development. *Eur J Clin Invest* 2015;**45**:100–108.
9. Makinen T, Veikkola T, Mustjoki S, Karpanen T, Catimel B, Nice EC, Wise L, Mercer A, Kowalski H, Kerjaschki D, Stacker SA, Achen MG, Alitalo K. Isolated lymphatic endothelial cells transduce growth, survival and migratory signals via the VEGF-C/D receptor VEGFR-3. *EMBO J* 2001;**20**:4762–4773.
10. Lin CY, Wang SW, Chen YL, Chou WY, Lin TY, Chen WC, Yang CY, Liu SC, Hsieh CC, Fong YC, Wang PC, Tang CH. Brain-derived neurotrophic factor promotes

VEGF-C-dependent lymphangiogenesis by suppressing miR-624-3p in human chondrosarcoma cells. *Cell Death Dis* 2017;**8**:e2964.
11. Lahdenranta J, Hagendoorn J, Padera TP, Hoshida T, Nelson G, Kashiwagi S, Jain RK, Fukumura D. Endothelial nitric oxide synthase mediates lymphangiogenesis and lymphatic metastasis. *Cancer Res* 2009;**69**:2801–2808.
12. Scallan JP, Hill MA, Davis MJ. Lymphatic vascular integrity is disrupted in type 2 diabetes due to impaired nitric oxide signalling. *Cardiovasc Res* 2015;**107**:89–97.
13. Grzegorek I, Drozdz K, Chmielewska M, Gomulkiewicz A, Jablonska K, Piotrowska A, Karczewski M, Janczak D, Podhorska-Okolow M, Dziegiel P, Szuba A. Arterial wall lymphangiogenesis is increased in the human iliac atherosclerotic arteries: involvement of CCR7 receptor. *Lymphat Res Biol* 2014;**12**:222–231.
14. Bornstein P. Matricellular proteins: an overview. *J Cell Commun Signal* 2009;**3**:163–165.
15. Csanyi G, Yao M, Rodriguez AI, Al Ghouleh I, Sharifi-Sanjani M, Frazziano G, Huang X, Kelley EE, Isenberg JS, Pagano PJ. Thrombospondin-1 regulates blood flow via CD47 receptor-mediated activation of NADPH oxidase 1. *Arterioscler Thromb Vasc Biol* 2012;**32**:2966–2973.
16. Hsu PL, Chen JS, Wang CY, Wu HL, Mo FE. Shear-induced CCN1 promotes atheroprone endothelial phenotypes and atherosclerosis. *Circulation* 2019;**139**:2877–2891.
17. Moura R, Tjwa M, Vandervoort P, Van Kerckhoven S, Holvoet P, Hoylaerts MF. Thrombospondin-1 deficiency accelerates atherosclerotic plaque maturation in ApoE-/- mice. *Circ Res* 2008;**103**:1181–1189.
18. Kim KA, Zhao J, Andarmani S, Kakitani M, Oshima T, Binnerts ME, Abo A, Tomizuka K, Funk WD. R-Spondin proteins: a novel link to beta-catenin activation. *Cell Cycle* 2006;**5**:23–26.
19. de Lau W, Barker N, Low TY, Koo BK, Li VS, Teunissen H, Kujala P, Haegebarth A, Peters PJ, van de Wetering M, Stange DE, van Es JE, Guardavaccaro D, Schasfoort RB, Mohri Y, Nishimori K, Mohammed S, Heck AJ, Clevers H. Lgr5 homologues associate with Wnt receptors and mediate R-spondin signalling. *Nature* 2011;**476**:293–297.
20. Carmon KS, Gong X, Lin Q, Thomas A, Liu Q. R-spondins function as ligands of the orphan receptors LGR4 and LGR5 to regulate Wnt/beta-catenin signaling. *Proc Natl Acad Sci USA* 2011;**108**:11452–11457.
21. Tan B, Shi X, Zhang J, Qin J, Zhang N, Ren H, Qian M, Siwko S, Carmon K, Liu Q, Han H, Du B, Liu M. Inhibition of Rspo-Lgr4 facilitates checkpoint blockade therapy by switching macrophage polarization. *Cancer Res* 2018;**78**:4929–4942.
22. Kazanskaya O, Ohkawara B, Heroult M, Wu W, Maltry N, Augustin HG, Niehrs C. The Wnt signaling regulator R-spondin 3 promotes angioblast and vascular development. *Development* 2008;**135**:3655–3664.
23. Gore AV, Swift MR, Cha YR, Lo B, McKinney MC, Li W, Castranova D, Davis A, Mukouyama YS, Weinstein BM. Rspo1/Wnt signaling promotes angiogenesis via Vegfc/Vegfr3. *Development* 2011;**138**:4875–4886.
24. Munguía-Reyes A, Balderas-Martínez YI, Becerril C, Checa M, Ramírez R, Ortiz B, Meléndez-Zajgla J, Pardo A, Selman M. R-Spondin-2 is upregulated in idiopathic pulmonary fibrosis and affects fibroblast behavior. *Am J Respir Cell Mol Biol* 2018;**59**:65–76.
25. Sartore S, Chiavegato A, Faggin E, Franch R, Puato M, Ausoni S, Pauletto P. Contribution of adventitial fibroblasts to neointima formation and vascular remodeling: from innocent bystander to active participant. *Circ Res* 2001;**89**:1111–1121.
26. Dong X, Liao W, Zhang L, Tu X, Hu J, Chen T, Dai X, Xiong Y, Liang W, Ding C, Liu R, Dai J, Wang O, Lu L, Lu X. RSPO2 suppresses colorectal cancer metastasis by counteracting the Wnt5a/Fzd7-driven noncanonical Wnt pathway. *Cancer Lett* 2017;**402**:153–165.
27. Gomes FG, Nedel F, Alves AM, Nor JE, Tarquinio SB. Tumor angiogenesis and lymphangiogenesis: tumor/endothelial crosstalk and cellular/microenvironmental signaling mechanisms. *Life Sci* 2013;**92**:101–107.
28. Yang Q, Xu J, Ma Q, Liu Z, Sudhahar V, Cao Y, Wang L, Zeng X, Zhou Y, Zhang M, Xu Y, Wang Y, Weintraub NL, Zhang C, Fukai T, Wu C, Huang L, Han Z, Wang T, Fulton DJ, Hong M, Huo Y. PRKAA1/AMPKalpha1-driven glycolysis in endothelial cells exposed to disturbed flow protects against atherosclerosis. *Nat Commun* 2018;**9**:4667.
29. Kritz AB, Yu J, Wright PL, Wan S, George SJ, Halliday C, Kang N, Sessa WC, Baker AH. In vivo modulation of Nogo-B attenuates neointima formation. *Mol Ther* 2008;**16**:1798–1804.
30. Bjørklund MM, Hollensen AK, Hagensen MK, Dagnæs-Hansen F, Christoffersen C, Mikkelsen JG, Bentzon JF. Induction of atherosclerosis in mice and hamsters without germline genetic engineering. *Circ Res* 2014;**114**:1684–1689.
31. Singla B, Lin H-P, Ghoshal P, Cherian-Shaw M, Csányi G. PKCdelta stimulates macropinocytosis via activation of SSH1-cofilin pathway. *Cell Signal* 2019;**53**:111–121.
32. Takeda K, Sowa Y, Nishino K, Itoh K, Fushiki S. Adipose-derived stem cells promote proliferation, migration, and tube formation of lymphatic endothelial cells in vitro by secreting lymphangiogenic factors. *Ann Plast Surg* 2015;**74**:728–736.
33. Song L, Ding S, Ge Z, Zhu X, Qiu C, Wang Y, Lai E, Yang W, Sun Y, Chow SA, Yu L. Nucleoside/nucleotide reverse transcriptase inhibitors attenuate angiogenesis and lymphangiogenesis by impairing receptor tyrosine kinases signalling in endothelial cells. *Br J Pharmacol* 2018;**175**:1241–1259.
34. Wu H, Rahman HNA, Dong Y, Liu X, Lee Y, Wen A, To KHT, Xiao L, Birsner AE, Bazinet L, Wong S, Song K, Brophy ML, Mahamud MR, Chang B, Cai X, Pasula S, Kwak S, Yang W, Bischoff J, Xu J, Bielenberg DR, Dixon JB, D'Amato RJ, Srinivasan RS, Chen H. Epsin deficiency promotes lymphangiogenesis through regulation of VEGFR3 degradation in diabetes. *J Clin Invest* 2018;**128**:4025–4043.
35. Nisimoto Y, Jackson HM, Ogawa H, Kawahara T, Lambeth JD. Constitutive NADPH-dependent electron transferase activity of the Nox4 dehydrogenase domain. *Biochemistry* 2010;**49**:2433–2442.
36. Wu C, Qiu S, Lu L, Zou J, Li WF, Wang O, Zhao H, Wang H, Tang J, Chen L, Xu T, Sun Z, Liao W, Luo G, Lu X. RSPO2-LGR5 signaling has tumour-suppressive activity in colorectal cancer. *Nat Commun* 2014;**5**:3149.
37. Wu L, Zhang W, Qian J, Wu J, Jiang L, Ling C. R-spondin family members as novel biomarkers and prognostic factors in lung cancer. *Oncol Lett* 2019;**18**:4008–4015.
38. Chiu JJ, Chien S. Effects of disturbed flow on vascular endothelium: pathophysiological basis and clinical perspectives. *Physiol Rev* 2011;**91**:327–387.
39. Herbst RS, Oh Y, Wagle A, Lahn M. Enzastaurin, a protein kinase Cbeta-selective inhibitor, and its potential application as an anticancer agent in lung cancer. *Clin Cancer Res* 2007;**13**:s4641–s4646.
40. Partovian C, Zhuang Z, Moodie K, Lin M, Ouchi N, Sessa WC, Walsh K, Simons M. PKCalpha activates eNOS and increases arterial blood flow in vivo. *Circ Res* 2005;**97**:482–487.
41. Tai HC, Lee TH, Tang CH, Chen LP, Chen WC, Lee MS, Chen PC, Lin CY, Chi CW, Chen YJ, Lai CT, Chen SS, Liao KW, Lee CH, Wang SW. Phomaketide A inhibits lymphangiogenesis in human lymphatic endothelial cells. *Mar Drugs* 2019;**17**:215.
42. Shimizu Y, Shibata R, Ishii M, Ohashi K, Kambara T, Uemura Y, Yuasa D, Kataoka Y, Kihara S, Murohara T, Ouchi N. Adiponectin-mediated modulation of lymphatic vessel formation and lymphedema. *J Am Heart Assoc* 2013;**2**:e000438.
43. Knight MN, Karuppaiah K, Lowe M, Mohanty S, Zondervan RL, Bell S, Ahn J, Hankenson KD. R-spondin-2 is a Wnt agonist that regulates osteoblast activity and bone mass. *Bone Res* 2018;**6**:24.
44. Liu S, U KP, Zhang J, Tsang LL, Huang J, Tu SP, Jiang X. R-spodin2 enhances canonical Wnt signaling to maintain the stemness of glioblastoma cells. *Cancer Cell Int* 2018;**18**:156.
45. Conboy CB, Velez-Reyes GL, Tschida BR, Hu H, Kaufmann G, Koes N, Keller B, Alsinet C, Cornella H, Pinyol R, Abrahante JE, Temiz NA, Linden MA, Amin K, Kuka TP, Keng VW, Llovet JM, Starr TK, Largaespada DA. R-spondin 2 drives liver tumor development in a yes-associated protein-dependent manner. *Hepatol Commun* 2019;**3**:1496–1509.
46. Carmon KS, Gong X, Yi J, Thomas A, Liu Q. RSPO-LGR4 functions via IQGAP1 to potentiate Wnt signaling. *Proc Natl Acad Sci USA* 2014;**111**:E1221–E1229.
47. Du Q, Zhang X, Liu Q, Zhang X, Bartels CE, Geller DA. Nitric oxide production upregulates Wnt/beta-catenin signaling by inhibiting Dickkopf-1. *Cancer Res* 2013;**73**:6526–6537.
48. Cha B, Geng X, Mahamud MR, Zhang JY, Chen L, Kim W, Jho EH, Kim Y, Choi D, Dixon JB, Chen H, Hong YK, Olson L, Kim TH, Merrill BJ, Davis MJ, Srinivasan RS. Complementary Wnt sources regulate lymphatic vascular development via PROX1-dependent Wnt/beta-catenin signaling. *Cell Rep* 2018;**25**:571–584.e575.
49. Subramanian P, Karshovska E, Reinhard P, Megens RT, Zhou Z, Akhtar S, Schumann U, Li X, van Zandvoort M, Ludin C, Weber C, Schober A. Lysophosphatidic acid receptors LPA1 and LPA3 promote CXCL12-mediated smooth muscle progenitor cell recruitment in neointima formation. *Circ Res* 2010;**107**:96–105.
50. Huang L, Chambliss KL, Gao X, Yuhanna IS, Behling-Kelly E, Bergaya S, Ahmed M, Michaely P, Luby-Phelps K, Darehshouri A, Xu L, Fisher EA, Ge WP, Mineo C, Shaul PW. SR-B1 drives endothelial cell LDL transcytosis via DOCK4 to promote atherosclerosis. *Nature* 2019;**569**:565–569.
51. Lopez Gelston CA, Balasubbramanian D, Abouelkheir GR, Lopez AH, Hudson KR, Johnson ER, Muthuchamy M, Mitchell BM, Rutkowski JM. Enhancing renal lymphatic expansion prevents hypertension in mice. *Circ Res* 2018;**122**:1094–1101.
52. Chakraborty A, Barajas S, Lammoglia GM, Reyna AJ, Morley TS, Johnson JA, Scherer PE, Rutkowski JM. Vascular endothelial growth factor-D (VEGF-D) overexpression and lymphatic expansion in murine adipose tissue improves metabolism in obesity. *Am J Pathol* 2019;**189**:924–939.
53. Hasegawa S, Nakano T, Torisu K, Tsuchimoto A, Eriguchi M, Haruyama N, Masutani K, Tsuruya K, Kitazono T. Vascular endothelial growth factor-C ameliorates renal interstitial fibrosis through lymphangiogenesis in mouse unilateral ureteral obstruction. *Lab Invest* 2017;**97**:1439–1452.
54. Milasan A, Smaani A, Martel C. Early rescue of lymphatic function limits atherosclerosis progression in Ldlr(-/-) mice. *Atherosclerosis* 2019;**283**:106–119.
55. Masoudkabir F, Sarrafzadegan N, Gotay C, Ignaszewski A, Krahn AD, Davis MK, Franco C, Mani A. Cardiovascular disease and cancer: evidence for shared disease pathways and pharmacologic prevention. *Atherosclerosis* 2017;**263**:343–351.
56. Nagano K. R-spondin signaling as a pivotal regulator of tissue development and homeostasis. *Jpn Dent Sci Rev* 2019;**55**:80–87.
57. Vuorio T, Nurmi H, Moulton K, Kurkipuro J, Robciuc MR, Ohman M, Heinonen SE, Samaranayake H, Heikura T, Alitalo K, Yla-Herttuala S. Lymphatic vessel insufficiency in hypercholesterolemic mice alters lipoprotein levels and promotes atherogenesis. *Arterioscler Thromb Vasc Biol* 2014;**34**:1162–1170.

58. Klotz L, Norman S, Vieira JM, Masters M, Rohling M, Dube KN, Bollini S, Matsuzaki F, Carr CA, Riley PR. Cardiac lymphatics are heterogeneous in origin and respond to injury. *Nature* 2015;**522**:62–67.
59. Yan H, Zhang C, Wang Z, Tu T, Duan H, Luo Y, Feng J, Liu F, Yan X. CD146 is required for VEGF-C-induced lymphatic sprouting during lymphangiogenesis. *Sci Rep* 2017;**7**:7442.
60. Nakao S, Zandi S, Hata Y, Kawahara S, Arita R, Schering A, Sun D, Melhorn MI, Ito Y, Lara-Castillo N, Ishibashi T, Hafezi-Moghadam A. Blood vessel endothelial VEGFR-2 delays lymphangiogenesis: an endogenous trapping mechanism links lymph- and angiogenesis. *Blood* 2011;**117**:1081–1090.
61. Coso S, Zeng Y, Opeskin K, Williams ED. Vascular endothelial growth factor receptor-3 directly interacts with phosphatidylinositol 3-kinase to regulate lymphangiogenesis. *PLoS One* 2012;**7**:e39558.
62. Siems WG, Brenke R, Beier A, Grune T. Oxidative stress in chronic lymphoedema. *QJM* 2002;**95**:803–809.
63. Warboys CM, Chen N, Zhang Q, Shaifta Y, Vanderslott G, Passacquale G, Hu Y, Xu Q, Ward JP, Ferro A. Bidirectional cross-regulation between the endothelial nitric oxide synthase and beta-catenin signalling pathways. *Cardiovasc Res* 2014;**104**:116–126.
64. Bandara N, Gurusinghe S, Lim SY, Chen H, Chen S, Wang D, Hilbert B, Wang LX, Strappe P. Molecular control of nitric oxide synthesis through eNOS and caveolin-1 interaction regulates osteogenic differentiation of adipose-derived stem cells by modulation of Wnt/beta-catenin signaling. *Stem Cell Res Ther* 2016;**7**:182.
65. Nam JS, Park E, Turcotte TJ, Palencia S, Zhan X, Lee J, Yun K, Funk WD, Yoon JK. Mouse R-spondin2 is required for apical ectodermal ridge maintenance in the hindlimb. *Dev Biol* 2007;**311**:124–135.
66. Li Z, Liu S, Lou J, Mulholland M, Zhang W. LGR4 protects hepatocytes from injury in mouse. *Am J Physiol Gastrointest Liver Physiol* 2019;**316**:G123–G131.
67. Hu YW, Guo FX, Xu YJ, Li P, Lu ZF, McVey DG, Zheng L, Wang Q, Ye JH, Kang CM, Wu SG, Zhao JJ, Ma X, Yang Z, Fang FC, Qiu YR, Xu BM, Xiao L, Wu Q, Wu LM, Ding L, Webb TR, Samani NJ, Ye S. Long noncoding RNA NEXN-AS1 mitigates atherosclerosis by regulating the actin-binding protein NEXN. *J Clin Invest* 2019;**129**:1115–1128.

Translational perspective

Atherosclerotic cardiovascular disease is the leading cause of death worldwide. Thus, attenuation of atherosclerotic lesion formation and prevention of its cardiovascular complications is an urgent medical need. The findings of the present study may provide a framework from which novel therapeutic strategies to augment lymphatic vessel density and reduce atherosclerotic lesion formation can be developed. These results may also have important implications in other pathological conditions associated with lymphatic dysfunction, such as lymphedema, obesity, hypertension, and impaired wound healing.